# Chapter 5

# Signal region optimisation

In order to discover the rare SUSY signals considered in the following, dedicated kinematic regions enriched in signal events, so called signal regions (SRs) are constructed. They are optimised such as to be sensitive to a maximum number of signal models considered in the analysis. In this chapter, the optimisation procedures leading to the final signal regions are introduced and discussed.

## 5.1 Optimisation methods

All optimisation methods used in the following require a figure of merit that is maximised in order to find configurations yielding best performance. While the multidimensional cut scan and the $N-1$ plots approach introduced in in sections 5.1.1 and 5.1.2, respectively, use the binomial discovery significance $Z_{\mathrm{B}}$, the fit scan procedure discussed in section 5.1.3 aims to maximise the area of the expected exclusion contour.

### 5.1.1 Multidimensional cut scan

The first optimisation method used for designing the SRs is an $N$-dimensional cut[†] scan using $N$ observables. For each unique combination of requirements on the set of observables considered, the expected signal and background rate as well as the statistical uncertainty on the background rate is determined from the MC simulated events. As this takes a considerable computational effort, it is crucial to restrict the amount of cut combinations to be tested. By comparing with distributions at preselection level, as for example those shown in fig. 4.3, a set of discrete cuts can be defined for each observable. In practice, a total number of $\mathcal{O}(10^7$–$10^8)$ cut combinations can still be tested on a single machine with a reasonable turnaround time.

After determining the expected event rates and statistical uncertainties, the different cut combinations are binned into a predefined number of signal efficiency bins. For each bin, the background rejection is subsequently maximised, i.e. the cut combination with the highest background rejection is chosen as a candidate combination for the respective signal efficiency bin.

[†] In the following, the term *cut* refers to a simple upper or lower requirement on kinematic observables like e.g. requiring $m_{\mathrm{T}} > 100\,\mathrm{GeV}$.

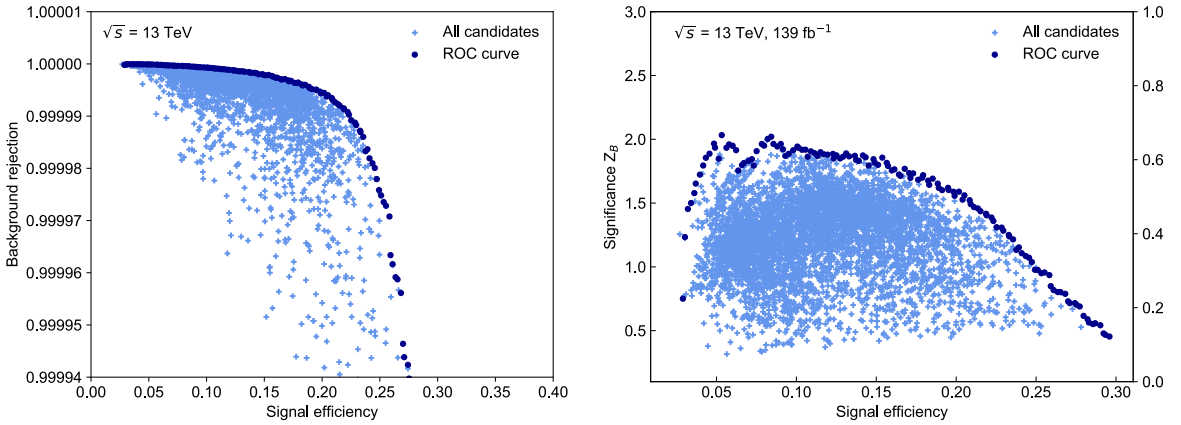


**(a)** **(b)**

**Figure 5.1:** Small $N$-dimensional cut scan using $10^4$ unique cut combinations, illustrating the approach of (a) generating a receiver operating characteristic (ROC) curve from the scanned cut combinations in order to (b) reduce the number of candidates used in computationally expensive significance calculations. The cut combination candidates forming the ROC curve (dark blue) also maximise the discovery significance. In (b), the significance $Z_B$ includes the MC statistical uncertainty on the expected background rate as well as 30% flat systematic uncertainty.

The assumption is that, for a fixed signal efficiency, the cut combination candidate maximising the background rejection also maximises the discovery significance $Z_B$. With the significance definition used herein, this is in general a valid assumption, as the significance tends to monotonically increase with decreasing background rate, even while the statistical uncertainty on the background estimation increases due to tighter requirements and less available MC statistics (cf. fig. 5.1). This procedure effectively generates a ROC curve, that can be used to perform more computationally intensive calculations, as e.g. calculating different variations of the discovery significance. The approach is illustrated in a small scan using $10^4$ cut combinations in fig. 5.1. The cut combination candidates maximising the background rejection and thus lying on the ROC curve in fig. 5.1(a) are the same candidates that maximise the discovery significance in fig. 5.1(b).

A common problem of $N$-dimensional scans is the concept of *overtightening* the selections given the available MC statistics. Since the cross sections of the SUSY process considered are many orders of magnitude smaller than those of the dominant SM processes, it is often necessary to apply tight requirements on the kinematic observables in order to achieve a significant signal-to-background separation. However, due to the finite amount of MC statistics available, many of the more extreme cut combinations select kinematic regions where not enough MC statistics are available for a reasonable estimation of the background rates. Thus, by maximising the background rejection, it may occur that cut combinations are selected where the mere lack of MC statistics, needed to properly estimate the background rates, causes a high significance value. As the significance values obtained for such configurations are obviosuly not trustworthy, they need to be avoided.

In the $N$-dimensional cut scan implementation used herein, the available MC datasets are split in two statistically independent, equally sized subsets. Although resulting in an additional dilution

of the available MC statistics, this approach allows to generate two independent ROC curves and to compute two independent values for the discovery significance for each cut combination candidate. A large difference in either the ROC curves or the significance values is an indication for statistical fluctuations as a result of overtightened cuts. In addition, requirements on the minimum number of unweighted MC events for different background processes, as well as the maximum allowed statistical uncertainty on a given process, can be applied. In combination, these precautions offer a good handle against statistical fluctuations. In the following, the $N$-dimensional cut scan implementation provided by AHOI [236] is used.

### 5.1.2 N-1 plots

Instead of performing a brute-force scan of a large set of cut combinations, a more manual approach, using iterative one-dimensional scans can be employed. In so-called '$N-1$ plots', the kinematic distributions of the background components as well as exemplary signal processes are plotted in conjunction with the significance achieved by applying a cut on each value on the $x$-axis of the one-dimensional distribution plotted. All other selection requirements, except the one on the observable plotted, are applied. This method allows to investigate the impact of a single kinematic requirement on the overall significance value. By repeatedly executing this process for each observable considered, it is possible to iteratively approach a cut combination yielding results comparable to that of a brute-force cut scan. Especially when considering a sizeable set of observables, this manual approach however quickly becomes very cumbersome and inefficient, and risks missing optimal cut combinations that would have been found by a brute-force approach.

For this reason, the following optimisation uses an $N$-dimensional cut scan to cover the full space spanned by the observables and scan ranges considered, while $N-1$ plots are used to verify and fine-tune results obtained by the brute-force approach.

### 5.1.3 Scans using asymptotic formulae

The last of the optimisation methods used in the following relies on scans over sets of simplified fit setups in order to run a simplified version of the full statistical inference machinery on a large number of signal region candidates. While the preceding optimisation methods rely on the binomial significance computed in independent cut-and-count signal regions, the simplified fit scans statistically combine disjunct signal regions by building a single likelihood, and compute the $p$-values using the asymptotic formulae introduced in chapter 3. In addition, the simplified fits use all available signal points instead of relying on a limited set of benchmark points, and can thus derive an estimate of the expected exclusion contour for a large number of signal region candidates. The estimation of the background event rates in the signal regions is taken from MC simulation only and considers a flat systematic uncertainty of 30% on the estimated event rate, correlated over all signal region bins. Statistical uncertainties on the background estimate from limited MC statistics are also taken into account.

As building the likelihood and executing the statistical inference takes a considerable computational effort, this method benefits from the previous optimisation steps defining promising signal region candidates worth scanning over. In order to keep the number of configurations to be tested at a manageable level, the signal region candidates obtained from the previous

**Table 5.1:** List of observables and cut ranges used in the $N$-dimensional cut scan. All cuts are optional and allowed not to be applied at all.

| Observable | | Cut values |
|---|---|---|
| $E_{\mathrm{T}}^{\mathrm{miss}}$ [GeV] | $>$ | $\in \{200, 220, 240, 260, 280, 300, 320, 340\}$ |
| $E_{\mathrm{T}}^{\mathrm{miss}}$ significance $\mathcal{S}$ | $>$ | $\in \{5, 10, 15\}$ |
| $m_{\mathrm{T}}$ [GeV] | $>$ | $\in \{100, 120, 140, 160, 180, 200, 220, 240, 260, 280, 300\}$ |
| $m_{\mathrm{CT}}$ [GeV] | $>$ | $\in \{100, 120, 140, 160, 180, 200, 220, 240, 260, 280, 300\}$ |
| $m_{b\bar{b}}$ lower [GeV] | $>$ | $\in \{85, 90, 95, 100, 105, 110, 115\}$ |
| $m_{b\bar{b}}$ upper [GeV] | $<$ | $\in \{130, 135, 140, 145, 150\}$ |
| $p_{\mathrm{T}}^{\ell}$ [GeV] | $>$ | $\in \{20, 40, 60, 80\}$ |
| $p_{\mathrm{T}}^{\mathrm{jet1}}$ [GeV] | $>$ | $\in \{50, 100, 150\}$ |
| $p_{\mathrm{T}}^{\mathrm{jet2}}$ [GeV] | $>$ | $\in \{50, 75, 100\}$ |
| $\Delta R_{jj}$ | $<$ | $\in \{0.8, 1.0, 1.2, 2.0\}$ |
| $\Delta R_{b\bar{b}}$ | $<$ | $\in \{0.8, 1.0, 1.2, 2.0\}$ |
| $N_{\mathrm{jet}}$ | $\leq$ | $\in \{2, 3, 4\}$ |
| $\Delta\phi(\boldsymbol{E}_{\mathrm{T}}^{\mathrm{miss}}, \boldsymbol{p}_{\mathrm{T}}^{\ell})$ [rad] | $>$ | $\in \{0.5, 1.0, 2.0, 2.5\}$ |

methods are only varied to a limited degree, assuming that they were already close to optimal to begin with.

## 5.2 Optimisation for the 1$\ell$ search

The optimisation of the signal regions for the 1$\ell$ search presented herein benefits from experience past analyses investigating the same simplified model in the same final state [167, 168], and explores new observables and signal region configurations optimised for the integrated luminosity of the full Run 2 dataset.

### 5.2.1 Starting from benchmark signal points

A total of six so-called *benchmark* signal points, each representative for a different part of the model parameter space, are chosen for the first step of the optimisation procedure involving $N$-dimensional cut scans and $N-1$ plots. Apart from the variables introduced in section 4.6, a set of additional, potentially discriminative observables are considered in the $N$-dimensional cut scan[†]:

- Transverse momenta of the two leading jets as well as the lepton ($p_{\mathrm{T}}^{\mathrm{jet1}}$, $p_{\mathrm{T}}^{\mathrm{jet2}}$, $p_{\mathrm{T}}^{\ell}$). Especially for signal models with high mass differences between the electroweakinos, the transverse momenta of the lepton and the jets tend to have higher values than in SM background processes.
- Object-based $E_{\mathrm{T}}^{\mathrm{miss}}$ significance $\mathcal{S}$ [237], a quantity designed to quantify how genuine the reconstructed $E_{\mathrm{T}}^{\mathrm{miss}}$ in an event is. It is determined through a hypothesis test using a log-likelihood ratio that takes into account the resolution of all objects entering the

[†] These variables will turn out not to be used for the final signal regions and are only introduced here for completeness of the optimisation procedure description.

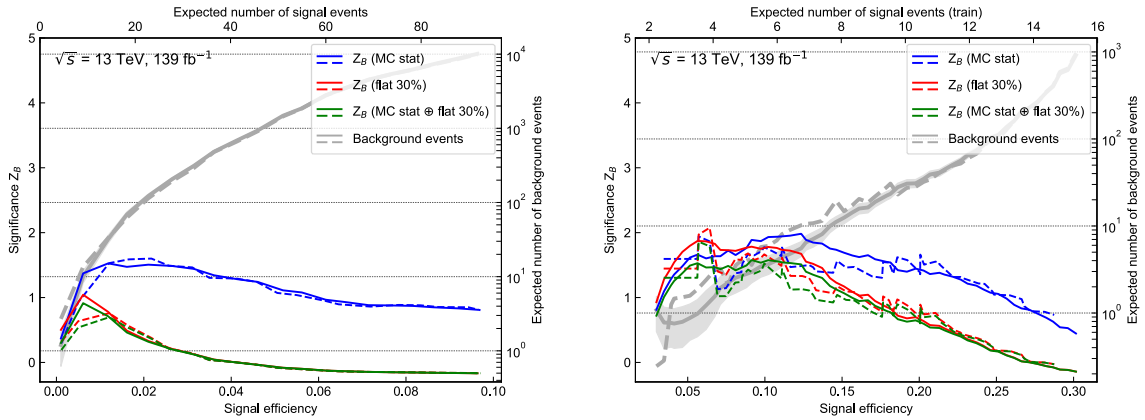


**(a)** $m(\tilde{\chi}_1^\pm/\tilde{\chi}_2^0), m(\tilde{\chi}_1^0) = 300, 150\,\text{GeV}$ **(b)** $m(\tilde{\chi}_1^\pm/\tilde{\chi}_2^0), m(\tilde{\chi}_1^0) = 800, 250\,\text{GeV}$

**Figure 5.2:** Results of the $N$-dimensional cut scan for two exemplary benchmark points. The binomial discovery significance $Z_\text{B}$ is plotted against the signal efficiency for different uncertainty configurations. Additionally, the expected SM background event rates are shown (grey), including their statistical uncertainty for one of the two statistically independent samples (grey shaded area). The solid and dashed lines represent the two statistically independent subsets that the MC samples are split into.

computation of $E_\text{T}^\text{miss}$. As such, $\mathcal{S}$ offers good discrimination against events with a sizeable fraction of fake $E_\text{T}^\text{miss}$ in the event originating e.g. from jet mismeasurements or the non-hermeticity of the detector. Events with a large share of fake $E_\text{T}^\text{miss}$ accumulate at low values of $\mathcal{S}$, while events with mostly real $E_\text{T}^\text{miss}$ tend to have large values of $\mathcal{S}$.

- The distance between the two leading jets $\Delta R_{jj}$ as well as the two $b$-jets $\Delta R_{b\bar{b}}$. Especially in events with a large mass difference between the electroweakinos, the Higgs can get a significant boost, such that the two $b$-jets from the Higgs decay tend to be close together in the laboratory frame (and are also the highest-$p_\text{T}$ jets in an event), resulting in small values of both $\Delta R_{jj}$ and $\Delta R_{b\bar{b}}$. In SM background processes, however, the two leading ($b$-)jets often do not originate from the same object and thus tend to be further apart.

- The azimuthal distance between the lepton $p_\text{T}$ and the missing transverse momentum, $\Delta\phi(\boldsymbol{p}_\text{T}^\ell, \boldsymbol{p}_\text{T}^\text{miss})$. This observable exploits the fact that the lepton and the $E_\text{T}^\text{miss}$ tend to have a more back-to-back configuration in signal events than in many SM processes where the lepton and the neutrino (the latter often responsible for a large part of the $E_\text{T}^\text{miss}$ in an event) often originate from the same $W$ boson decay.

In order to avoid selecting cut combination candidates with overtightened selection criteria compared to the available MC statistics, constraints on the relative statistical uncertainty on the background and on the number of unweighted MC events passing the cut combination candidates are applied. Cut combinations are only considered if they result in less than 50% relative statistical uncertainty on the total background. In addition, all cut combinations need to result in at least five unweighted MC events for each of the three major backgrounds, $t\bar{t}$, single top and $W$ + jets.

The discrete selection possibilities for each of the observables are shown in table 5.1. A preselection of one lepton and exactly two $b$-jets (and thus at least two jets overall in the event)

**Table 5.2:** Optimal cut combination for each benchmark signal point obtained with a brute force cut scan and a round of $N-1$ plots. The parameters of the benchmark points $m(\tilde{\chi}_1^{\pm}/\tilde{\chi}_2^0)$ and $m(\tilde{\chi}_1^0)$, both given in GeV. The significance is computed for 139 fb$^{-1}$ with the binomial discovery significance $Z_B$ and includes MC statistical uncertainty as well as a flat 30% systematic uncertainty. A dash '–' is used where no requirement on the respective observable is applied.

| Observable | $(300, 150)$ | $(400, 200)$ | $(600, 300)$ | $(800, 250)$ | $(800, 150)$ | $(800, 0)$ |
|---|---|---|---|---|---|---|
| $N_{b-\text{jet}}$ | 2 | 2 | 2 | 2 | 2 | 2 |
| $N_{\text{jet}}$ | 2 | 2 | 2 – 3 | 2 – 3 | 2 – 3 | 2 – 3 |
| $m_{b\bar{b}}$ [GeV] | $[105-135]$ | $[100-140]$ | $[100-140]$ | $[95-145]$ | $[95-145]$ | $[95-145]$ |
| $E_{\text{T}}^{\text{miss}}$ [GeV] | $> 240$ | $> 240$ | $> 240$ | $> 240$ | $> 240$ | $> 240$ |
| $m_{\text{CT}}$ [GeV] | $> 200$ | $> 240$ | $> 260$ | $> 260$ | $> 260$ | $> 280$ |
| $m_{\text{T}}$ [GeV] | $> 100$ | $> 120$ | $> 140$ | $> 200$ | $> 240$ | $> 240$ |
| $m_{\ell b_1}$ [GeV] | – | – | $> 150$ | $> 120$ | $> 120$ | $> 120$ |
| $Z_B$ $[\sigma]$ | 0.8 | 1.9 | 2.1 | 1.8 | 2.2 | 2.3 |

is always applied. Requirements on the different observables in table 5.1 are optional and do not need to be applied by the optimisation algorithm. The results of the brute-force $N$-dimensional cut scans for each benchmark signal point can be visualised by plotting the expected discovery significance $Z_B$ against the signal efficiency. Figure 5.2 shows the results of two such cut scans using two of the benchmark signal points. The corresponding plots for the remaining benchmark points are shown in fig. A.1. In these figures, the binomial significance is calculated for different uncertainty configurations for each of the two statistically independent subsets. In addition, the expected background rate is shown for each subset. A cut combination with high achieved significance can be chosen, while avoiding statistical fluctuations and overtightening. The cut combinations chosen for each benchmark point, after a round of $N-1$ plots, are shown in table 5.2. The $N-1$ plots, shown in figs. A.2 to A.7, are used to validate and fine-tune the cut values obtained through the cut scan and allow to identify and remove cuts on observables that do not contribute significantly to the achieved $Z_B$ value. From the 12 observables initially considered, only six (excluding the $b$-jet multiplicity technically not part of the scan) are part of the optimised cut combination candidates. The remaining observables turned out not to significantly improve the sensitivity and are therefore dropped in the following.

### 5.2.2 Towards final signal regions

The optimal cut combinations obtained for the benchmark signal points, shown in table 5.2, need to be consolidated into a finite set of signal region. From table 5.2, it can be concluded, that all benchmark points favour a common baseline selection including exactly two $b$-jets, possibly one additional light jet, a Higgs mass window requirement of roughly $m_{b\bar{b}} \in [100, 140]$ GeV, and $E_{\text{T}}^{\text{miss}} > 240$ GeV. The remaining requirements on $m_{\text{T}}$, $m_{\text{CT}}$ and $m_{\ell b_1}$ are however not easily consolidated into a single signal region, as they vastly differ depending on the model parameter space and kinematic regime represented by each benchmark point.

From the normalised distributions in fig. 4.3, it can already be seen that signal points from different kinematic regimes in the parameter space would in principle prefer different requirements on all three of these observables. Designing a single signal region that achieves optimal

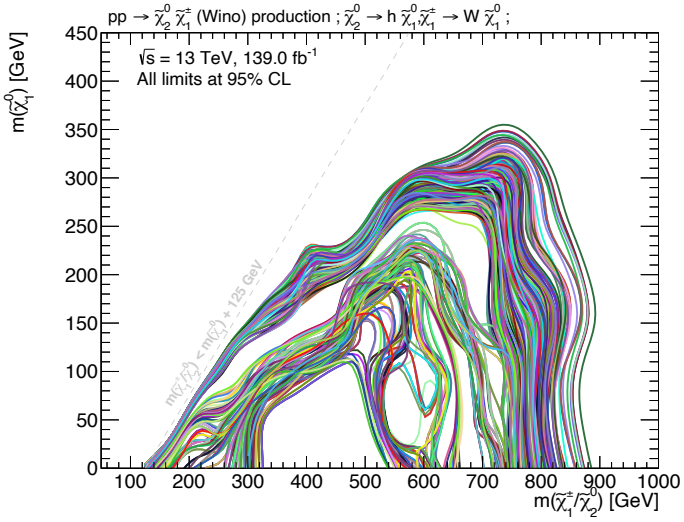


**Figure 5.3:** Expected exclusion contours obtained from a subset of the signal region candidates. The background estimation is taken directly from MC and includes MC statistical uncertainty as well as an uncorrelated shape uncertainty of 30%. For the sake of visibility, only the nominal contours are shown (without uncertainty bands). Configurations resulting in multiple, disjoint patches of excluded areas are rejected.

sensitivity to the entire parameter space studied, is thus not possible. Instead, a more generalised configuration is chosen, defining multiple signal region bins orthogonal to each other through their requirement on $m_{\mathrm{T}}$ and the $m_{\mathrm{CT}}$. Being mutually exclusive, such signal region bins can be statistically combined in a single likelihood, effectively creating a two-dimensional shape-fit in these observables as the different signal region bins can be fit simultaneously. Such a shape-fit configuration allows to exploit the differences in shape between signal and background distributions, and is able to accommodate the varying shapes of signal points from different regions in the parameter space, making it an ideal statistical tool to cover a wide range of kinematic regimes.

The optimal number of bins as well as values of the individual bin edges in both distributions depends on the available MC statistics and is determined using the simplified fit scans introduced in section 5.1.3. The MC statistical uncertainty as well as a systematic uncertainty of 30%, correlated over all bins, is considered in each scanned configuration. The number of bins are varied in each direction ($m_{\mathrm{T}}$ and $m_{\mathrm{CT}}$) between two and five and different bin edges, varying within ranges determined by the optimal cut values obtained for the benchmark points, are tested. As configurations with more bins could, in some circumstances, potentially benefit from the additional MC statistics resulting from looser selection criteria on the remaining variables, the previously consolidated baseline selection is also allowed to vary to some extent. Finally, although not expected to yield better performance, configurations with multiple orthogonal SR bins in the $E_{\mathrm{T}}^{\mathrm{miss}}$ or $m_{b\bar{b}}$ are also included in the scan. A subset of the investigated candidates are shown in fig. 5.3, only showing the nominal expected exclusion limit at 95% without uncertainty bands. Configurations with multiple, disjoint patches of excluded areas in the parameter space are discarded, as they typically result from high statistical fluctuations.

As expected from table 5.2, the best performing configurations define multiple signal region bins in the $m_{\mathrm{T}}$ and $m_{\mathrm{CT}}$ distributions, while keeping a constant baseline selection on the remaining observables. Figure 5.4(a) shows a comparison of the expected exclusion contour for exemplary two-dimensional shape-fit configurations, using signal regions binned in ($m_{\mathrm{T}}$, $E_{\mathrm{T}}^{\mathrm{miss}}$), ($m_{\mathrm{T}}$, $m_{b\bar{b}}$) or ($m_{\mathrm{T}}$, $m_{\mathrm{CT}}$). The setup using a two-dimensional shape-fit in $m_{\mathrm{T}}$ and $m_{\mathrm{CT}}$ clearly maximises the expected excluded area. In addition, this configuration also leads to optimal sensitivity within the expected limit, as is illustrated in fig. A.8(a). Finally, applying a requirement on

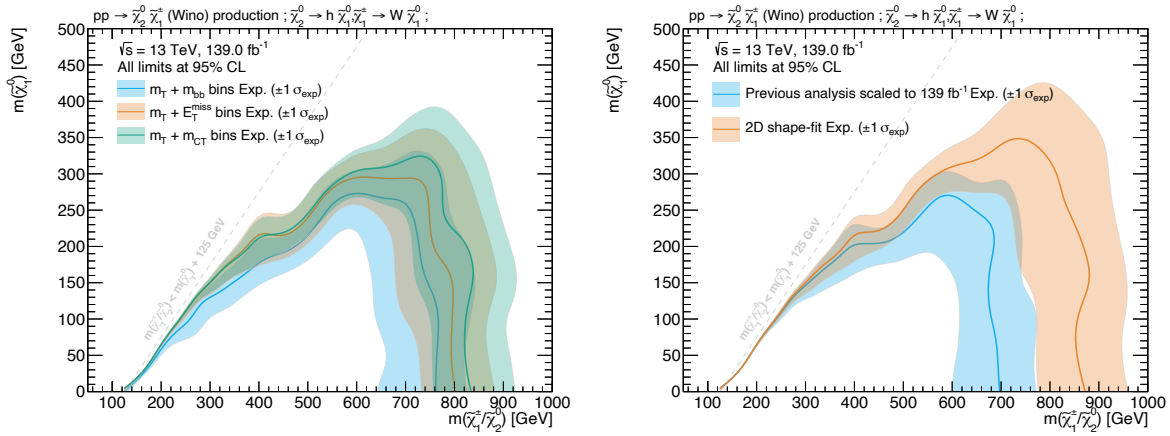


**(a)** **(b)**

**Figure 5.4:** Comparison of different shape-fit configurations. Fig. (a) compares three different two-dimensional shape-fit configurations using $3 \times 3$ bins in ($m_{\mathrm{T}}$, $E_{\mathrm{T}}^{\mathrm{miss}}$), ($m_{\mathrm{T}}$, $m_{b\bar{b}}$) and ($m_{\mathrm{T}}$, $m_{\mathrm{CT}}$). Fig. (b) compares the two-dimensional shape-fit in $m_{\mathrm{T}}$ and $m_{\mathrm{CT}}$ to the previous analysis iteration signal regions scaled to 139 fb$^{-1}$. All shown exclusion limits are expected limits at 95% CL, using MC statistical and 30% systematic uncertainty.

high values of $m_{\ell b_1}$ in the highest $m_{\mathrm{T}}$ bins has been shown (cf. fig. A.8(b)) to significantly improve sensitivity to signal models with high mass differences.

In fig. 5.4(b), the fully optimised two-dimensional shape-fit configuration is compared with the signal regions of the previous iteration of the search [168], scaled up to the integrated luminosity of the full Run 2 dataset. It can be seen that a significant improvement in sensitivity can be achieved through the introduction of the two-dimensional shape-fit strategy.

## 5.3 Signal region definitions

An overview of the final signal region definitions is provided in table 5.3. Based on the previously discussed results, three signal regions bins in $m_{\mathrm{T}}$ are defined, optimised for the low (SR-LM), medium (SR-MM), and high (SR-HM) mass difference regimes. While SR-LM targets the smallest values of $m_{\mathrm{T}}$, SR-MM and SR-HM target progressively increasing values of $m_{\mathrm{T}}$. All three signal regions are further divided into three $m_{\mathrm{CT}}$ bins each, resulting in a total of nine disjoint SR bins. The signal region with the highest requirement on $m_{\mathrm{T}}$ (SR-HM) also requires $m_{\ell b_1} > 120\,\mathrm{GeV}$, for the reason explained previously. All three SRs otherwise share a common set of requirements on the number of jets, $E_{\mathrm{T}}^{\mathrm{miss}}$ and $m_{b\bar{b}}$. As shape-fits are by construction highly model-dependent[†], these SRs will be used for deriving model-dependent limits in the case where no significant excess compared to the expected SM background rate is seen in data. For this reason, the shape-fit regions will be referred to as *exclusion* regions in the following. A graphical representation of the nine exclusion signal region bins is shown in fig. 5.5. The kinematic distributions in each SR-LM, SR-MM and SR-HM are shown as $N-1$ plots in figs. 5.6 to 5.8.

[†] The signal shapes need to be known in order to estimate the expected signal rates in multiple, disjoint signal region bins.

**Table 5.3:** Overview of the selection criteria for the signal regions. Exclusion SRs ('excl.') are defined for model-dependent limits, and discovery SRs ('disc.') are defined for model-independent upper limits. A dash '–' is used where no requirement on the respective observable is applied.

| | **SR-LM** | **SR-MM** | **SR-HM** |
|---|---|---|---|
| $N_{\text{lepton}}$ | $= 1$ | | |
| $p_{\text{T}}^{\ell}$ [GeV] | $> 7(6)$ for $e(\mu)$ | | |
| $N_{\text{jet}}$ | $= 2$ or 3 | | |
| $N_{b\text{-jet}}$ | $= 2$ | | |
| $E_{\text{T}}^{\text{miss}}$ [GeV] | $> 240$ | | |
| $m_{b\bar{b}}$ [GeV] | $\in [100, 140]$ | | |
| $m(\ell, b_1)$ [GeV] | – | – | $> 120$ |
| $m_{\text{T}}$ [GeV] (excl.) | $\in [100, 160]$ | $\in [160, 240]$ | $> 240$ |
| $m_{\text{CT}}$ [GeV] (excl.) | $\{\in [180, 230], \in [230, 280], > 280\}$ | | |
| $m_{\text{T}}$ [GeV] (disc.) | $> 100$ | $> 160$ | $> 240$ |
| $m_{\text{CT}}$ [GeV] (disc.) | $> 180$ | | |

For evaluating a potential excess in data compared to the expected background rate, a second set of signal regions is derived from the optimised shape-fit setup. For each of the three bins in the transverse mass (SR-LM, SR-MM, and SR-HM), the three $m_{\text{CT}}$ bins are summed up and the upper bound on $m_{\text{T}}$ is removed (if present). This results in three cut-and-count signal regions that make minimal model assumptions and can be interpreted in any BSM model, as long as the expected signal rates are known. In case no significant excess over the SM expectation is seen in data, these so-called *discovery* SRs can be used to derive model-independent upper limits on the visible cross section of BSM processes.

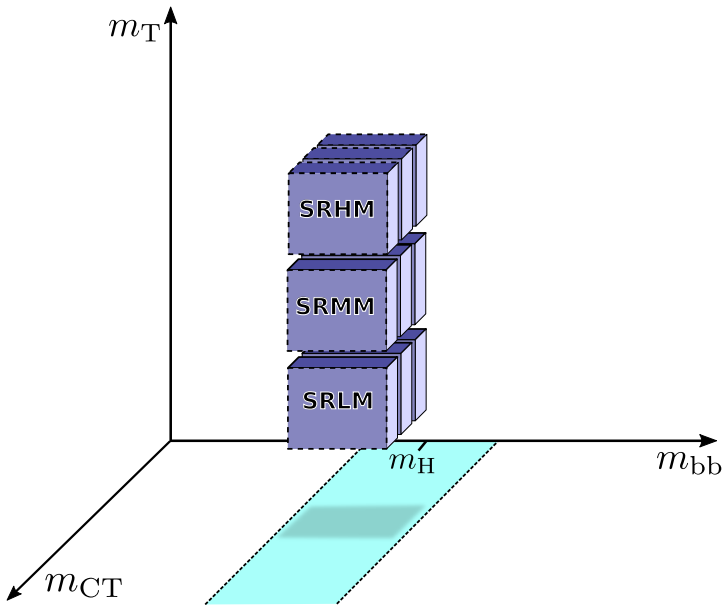


**Figure 5.5:** Configuration of the exclusion signal regions. Nine signal region bins are defined on $m_{\mathrm{T}}$ and $m_{\mathrm{CT}}$ within the Higgs mass window. All signal regions can be statistically combined using a single likelihood, effectively resulting in a two-dimensional shape-fit.

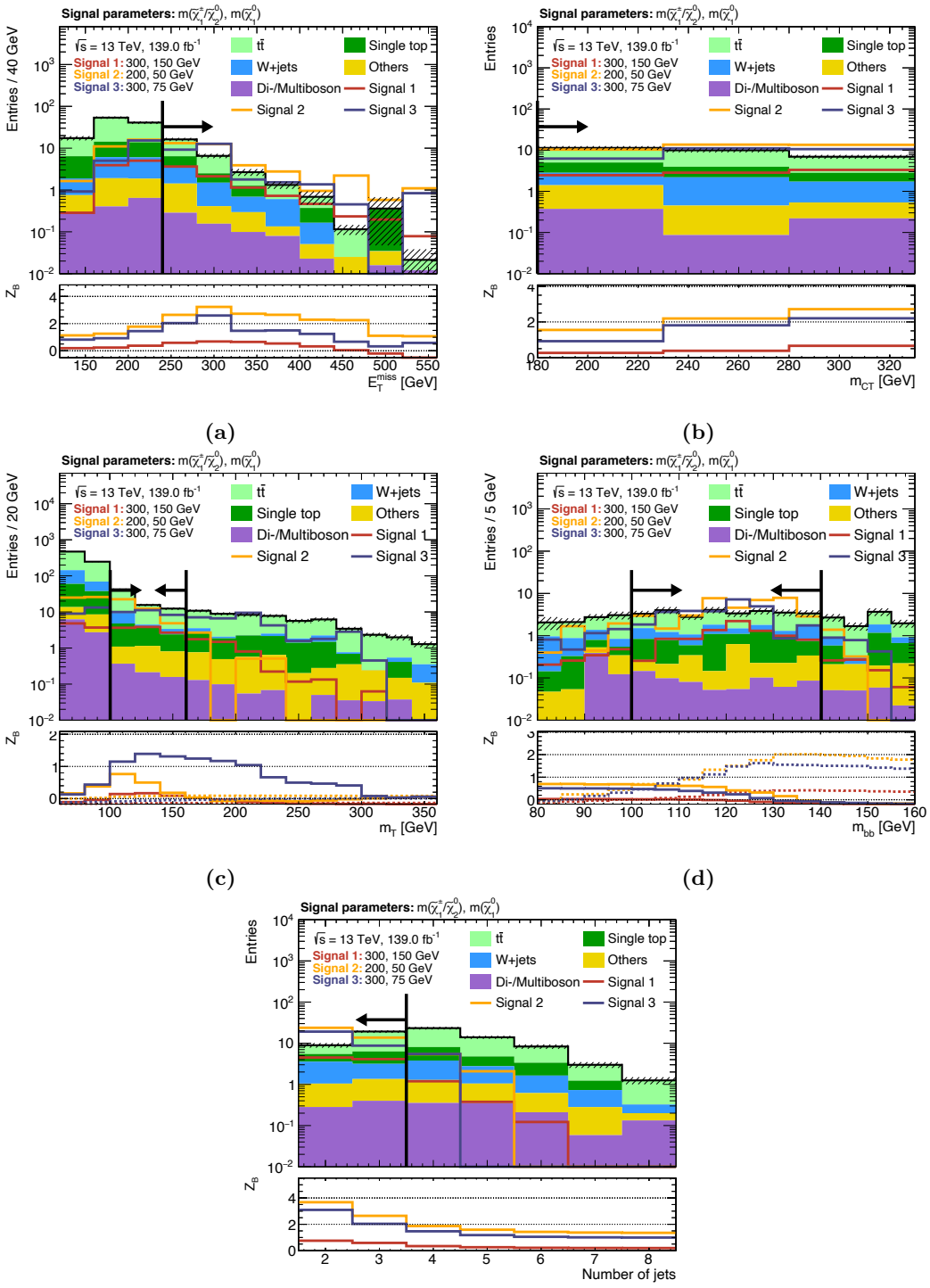


**Figure 5.6:** $N-1$ plots for SR-LM, with exemplary signal points and all $m_{\mathrm{CT}}$ bins included. The dashed area represents MC statistical uncertainty on the background. In all figures except fig. (b), the significance in the lower pad is obtained by summing up all the events in the direction of the cut arrow and includes 30% uncertainty as well as MC statistical uncertainty. In fig. (b) the significance is only computed on a bin-by-bin basis, i.e. not summing up all events in the direction of the cut arrow.

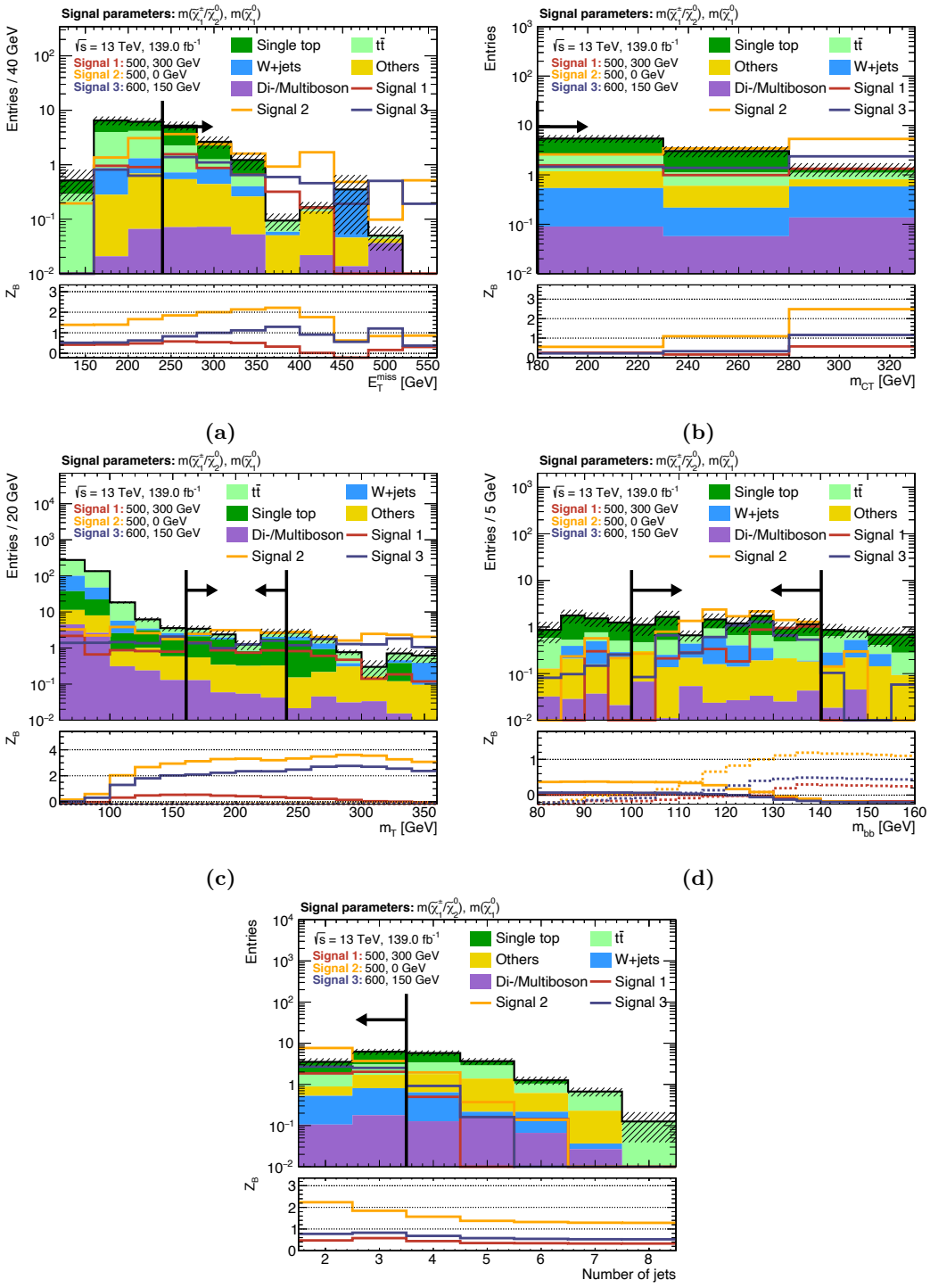


**Figure 5.7:** $N-1$ plots for SR-MM, with exemplary signal points and all $m_{\mathrm{CT}}$ bins included. The dashed area represents MC statistical uncertainty on the background. In all figures except fig. (b), the significance in the lower pad is obtained by summing up all the events in the direction of the cut arrow and includes 30% uncertainty as well as MC statistical uncertainty. In fig. (b) the significance is only computed on a bin-by-bin basis, i.e. not summing up all events in the direction of the cut arrow.

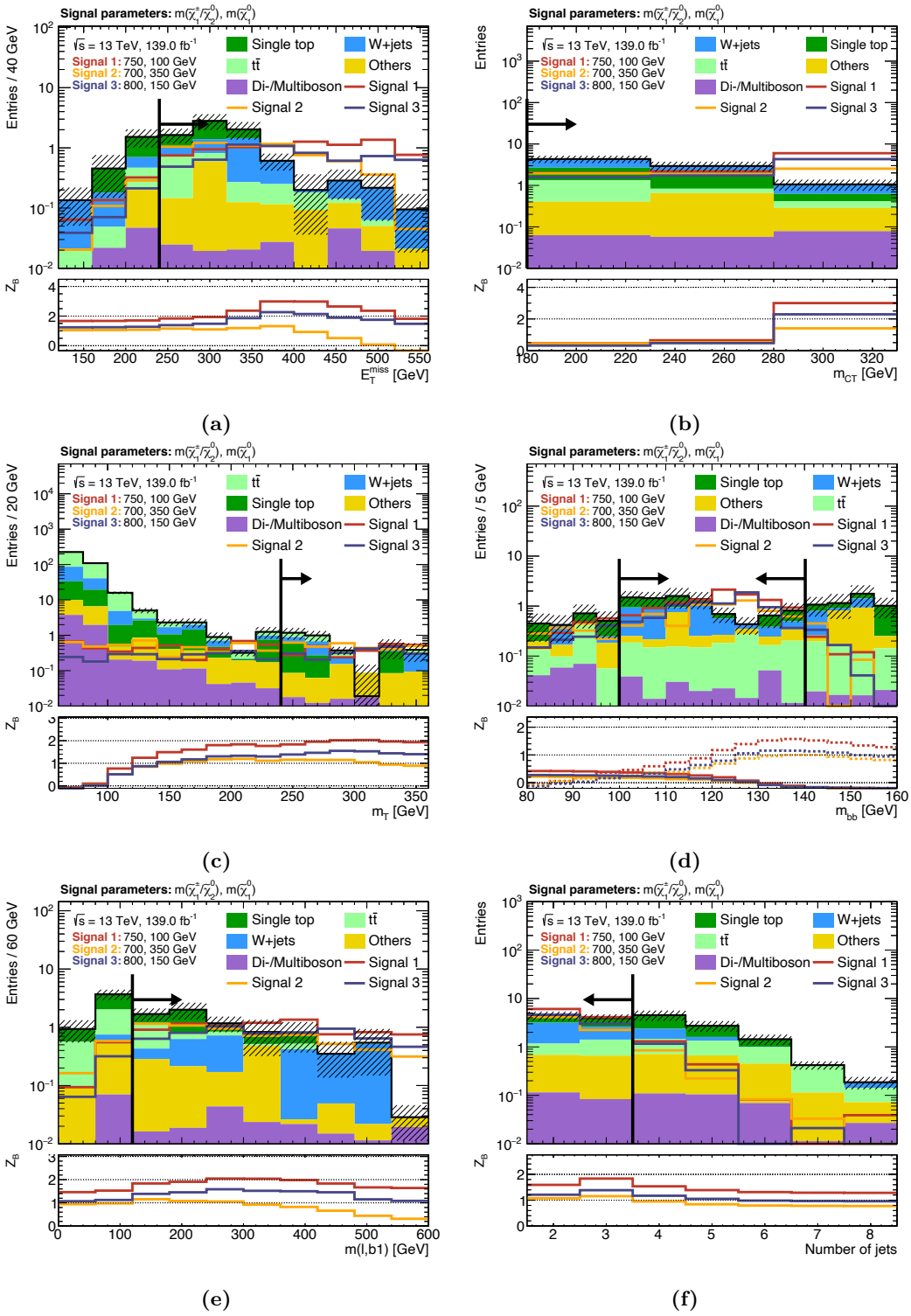


**Figure 5.8:** $N-1$ plots for SR-HM, with exemplary signal points and all $m_{\mathrm{CT}}$ bins included. The dashed area represents MC statistical uncertainty on the background. In all figures except fig. (b), the significance in the lower pad is obtained by summing up all the events in the direction of the cut arrow and includes 30% uncertainty as well as MC statistical uncertainty. In fig. (b) the significance is only computed on a bin-by-bin basis, i.e. not summing up all events in the direction of the cut arrow.

# Bibliography


[1] I. C. Brock and T. Schorner-Sadenius, *Physics at the terascale*. Wiley, Weinheim, 2011. https://cds.cern.ch/record/1354959.

[2] M. E. Peskin and D. V. Schroeder, *An Introduction to quantum field theory*. Addison-Wesley, Reading, USA, 1995. http://www.slac.stanford.edu/~mpeskin/QFT.html.

[3] S. P. Martin, "A Supersymmetry primer," arXiv:hep-ph/9709356 [hep-ph]. [Adv. Ser. Direct. High Energy Phys.18,1(1998)].

[4] M. Bustamante, L. Cieri, and J. Ellis, "Beyond the Standard Model for Montaneros," in *5th CERN - Latin American School of High-Energy Physics*. 11, 2009. arXiv:0911.4409 [hep-ph].

[5] L. Brown, *The Birth of particle physics*. Cambridge University Press, Cambridge Cambridgeshire New York, 1986.

[6] P. J. Mohr, D. B. Newell, and B. N. Taylor, "CODATA Recommended Values of the Fundamental Physical Constants: 2014," *Rev. Mod. Phys.* **88** no. 3, (2016) 035009, arXiv:1507.07956 [physics.atom-ph].

[7] P. D. Group, "Review of Particle Physics," *Progress of Theoretical and Experimental Physics* **2020** no. 8, (08, 2020) , https://academic.oup.com/ptep/article-pdf/2020/8/083C01/34673722/ptaa104.pdf. https://doi.org/10.1093/ptep/ptaa104. 083C01.

[8] **Super-Kamiokande** Collaboration, Y. Fukuda *et al.*, "Evidence for oscillation of atmospheric neutrinos," *Phys. Rev. Lett.* **81** (1998) 1562–1567, arXiv:hep-ex/9807003 [hep-ex].

[9] Z. Maki, M. Nakagawa, and S. Sakata, "Remarks on the unified model of elementary particles," *Prog. Theor. Phys.* **28** (1962) 870–880. [,34(1962)].

[10] N. Cabibbo, "Unitary symmetry and leptonic decays," *Phys. Rev. Lett.* **10** (Jun, 1963) 531–533. https://link.aps.org/doi/10.1103/PhysRevLett.10.531.

[11] M. Kobayashi and T. Maskawa, "CP Violation in the Renormalizable Theory of Weak Interaction," *Prog. Theor. Phys.* **49** (1973) 652–657.

[12] E. Noether and M. A. Tavel, "Invariant variation problems," arXiv:physics/0503066.

[13] J. C. Ward, "An identity in quantum electrodynamics," *Phys. Rev.* **78** (Apr, 1950) 182–182. https://link.aps.org/doi/10.1103/PhysRev.78.182.

[14] Y. Takahashi, "On the generalized ward identity," *Il Nuovo Cimento (1955-1965)* **6** no. 2, (Aug, 1957) 371–375. https://doi.org/10.1007/BF02832514.

[15] G. 'tHooft, "Renormalization of massless yang-mills fields," *Nuclear Physics B* **33** no. 1, (1971) 173 – 199. http://www.sciencedirect.com/science/article/pii/0550321371903956.

[16] J. Taylor, "Ward identities and charge renormalization of the yang-mills field," *Nuclear Physics B* **33** no. 2, (1971) 436 – 444. http://www.sciencedirect.com/science/article/pii/0550321371902975.

[17] A. A. Slavnov, "Ward identities in gauge theories," *Theoretical and Mathematical Physics* **10** no. 2, (Feb, 1972) 99–104. https://doi.org/10.1007/BF01090719.

[18] C. N. Yang and R. L. Mills, "Conservation of isotopic spin and isotopic gauge invariance," *Phys. Rev.* **96** (Oct, 1954) 191–195. https://link.aps.org/doi/10.1103/PhysRev.96.191.

[19] K. G. Wilson, "Confinement of quarks," *Phys. Rev. D* **10** (Oct, 1974) 2445–2459. https://link.aps.org/doi/10.1103/PhysRevD.10.2445.

[20] T. DeGrand and C. DeTar, *Lattice Methods for Quantum Chromodynamics*. World Scientific, Singapore, 2006. https://cds.cern.ch/record/1055545.

[21] S. L. Glashow, "Partial-symmetries of weak interactions," *Nuclear Physics* **22** no. 4, (1961) 579 – 588. http://www.sciencedirect.com/science/article/pii/0029558261904692.

[22] S. Weinberg, "A model of leptons," *Phys. Rev. Lett.* **19** (Nov, 1967) 1264–1266. https://link.aps.org/doi/10.1103/PhysRevLett.19.1264.

[23] A. Salam and J. C. Ward, "Weak and electromagnetic interactions," *Il Nuovo Cimento (1955-1965)* **11** no. 4, (Feb, 1959) 568–577. https://doi.org/10.1007/BF02726525.

[24] C. S. Wu, E. Ambler, R. W. Hayward, D. D. Hoppes, and R. P. Hudson, "Experimental test of parity conservation in beta decay," *Phys. Rev.* **105** (Feb, 1957) 1413–1415. https://link.aps.org/doi/10.1103/PhysRev.105.1413.

[25] M. Gell-Mann, "The interpretation of the new particles as displaced charge multiplets," *Il Nuovo Cimento (1955-1965)* **4** no. 2, (Apr, 1956) 848–866. https://doi.org/10.1007/BF02748000.

[26] K. Nishijima, "Charge Independence Theory of V Particles*," *Progress of Theoretical Physics* **13** no. 3, (03, 1955) 285–304, `https://academic.oup.com/ptp/article-pdf/13/3/285/5425869/13-3-285.pdf`. https://doi.org/10.1143/PTP.13.285.

[27] T. Nakano and K. Nishijima, "Charge Independence for V-particles*," *Progress of Theoretical Physics* **10** no. 5, (11, 1953) 581–582, `https://academic.oup.com/ptp/article-pdf/10/5/581/5364926/10-5-581.pdf`. https://doi.org/10.1143/PTP.10.581.

[28] F. Englert and R. Brout, "Broken symmetry and the mass of gauge vector mesons," *Phys. Rev. Lett.* **13** (Aug, 1964) 321–323. https://link.aps.org/doi/10.1103/PhysRevLett.13.321.

[29] P. W. Higgs, "Broken symmetries and the masses of gauge bosons," *Phys. Rev. Lett.* **13** (Oct, 1964) 508–509. https://link.aps.org/doi/10.1103/PhysRevLett.13.508.

[30] P. W. Higgs, "Spontaneous symmetry breakdown without massless bosons," *Phys. Rev.* **145** (May, 1966) 1156–1163. https://link.aps.org/doi/10.1103/PhysRev.145.1156.

[31] Y. Nambu, "Quasiparticles and Gauge Invariance in the Theory of Superconductivity," *Phys. Rev.* **117** (1960) 648–663. [,132(1960)].

[32] J. Goldstone, "Field Theories with Superconductor Solutions," *Nuovo Cim.* **19** (1961) 154–164.

[33] V. Brdar, A. J. Helmboldt, S. Iwamoto, and K. Schmitz, "Type-I Seesaw as the Common Origin of Neutrino Mass, Baryon Asymmetry, and the Electroweak Scale," *Phys. Rev. D* **100** (2019) 075029, arXiv:1905.12634 [hep-ph].

[34] G. 't Hooft and M. Veltman, "Regularization and renormalization of gauge fields," *Nuclear Physics B* **44** no. 1, (1972) 189 – 213. http://www.sciencedirect.com/science/article/pii/0550321372902799.

[35] F. Zwicky, "Die Rotverschiebung von extragalaktischen Nebeln," *Helv. Phys. Acta* **6** (1933) 110–127. https://cds.cern.ch/record/437297.

[36] V. C. Rubin and W. K. Ford, Jr., "Rotation of the Andromeda Nebula from a Spectroscopic Survey of Emission Regions," *Astrophys. J.* **159** (1970) 379–403.

[37] G. Bertone, D. Hooper, and J. Silk, "Particle dark matter: Evidence, candidates and constraints," *Phys. Rept.* **405** (2005) 279–390, arXiv:hep-ph/0404175.

[38] D. Clowe, M. Bradac, A. H. Gonzalez, M. Markevitch, S. W. Randall, C. Jones, and D. Zaritsky, "A direct empirical proof of the existence of dark matter," *Astrophys. J.* **648** (2006) L109–L113, arXiv:astro-ph/0608407 [astro-ph].

[39] A. Taylor, S. Dye, T. J. Broadhurst, N. Benitez, and E. van Kampen, "Gravitational lens magnification and the mass of abell 1689," *Astrophys. J.* **501** (1998) 539, arXiv:astro-ph/9801158.

[40] C. Bennett *et al.*, "Four year COBE DMR cosmic microwave background observations: Maps and basic results," *Astrophys. J. Lett.* **464** (1996) L1–L4, arXiv:astro-ph/9601067.

[41] G. F. Smoot *et al.*, "Structure in the COBE Differential Microwave Radiometer First-Year Maps," *ApJS* **396** (September, 1992) L1.

[42] **WMAP** Collaboration, "Nine-year Wilkinson Microwave Anisotropy Probe (WMAP) Observations: Final Maps and Results," *ApJS* **208** no. 2, (October, 2013) 20, arXiv:1212.5225 [astro-ph.CO].

[43] **WMAP** Collaboration, "Nine-year Wilkinson Microwave Anisotropy Probe (WMAP) Observations: Cosmological Parameter Results," *ApJS* **208** no. 2, (October, 2013) 19, arXiv:1212.5226 [astro-ph.CO].

[44] **Planck** Collaboration, "Planck 2018 results. I. Overview and the cosmological legacy of Planck," *Astron. Astrophys.* **641** (2020) A1, arXiv:1807.06205 [astro-ph.CO].

[45] A. Liddle, *An introduction to modern cosmology; 3rd ed.* Wiley, Chichester, Mar, 2015. https://cds.cern.ch/record/1976476.

[46] **Planck** Collaboration, "Planck 2018 results. VI. Cosmological parameters," *Astron. Astrophys.* **641** (2020) A6, arXiv:1807.06209 [astro-ph.CO].

[47] H. Georgi and S. L. Glashow, "Unity of all elementary-particle forces," *Phys. Rev. Lett.* **32** (Feb, 1974) 438–441. https://link.aps.org/doi/10.1103/PhysRevLett.32.438.

[48] I. Aitchison, *Supersymmetry in Particle Physics. An Elementary Introduction*. Cambridge University Press, Cambridge, 2007.

[49] **Muon g-2** Collaboration, G. Bennett *et al.*, "Final Report of the Muon E821 Anomalous Magnetic Moment Measurement at BNL," *Phys. Rev. D* **73** (2006) 072003, arXiv:hep-ex/0602035.

[50] H. Baer and X. Tata, *Weak Scale Supersymmetry: From Superfields to Scattering Events*. Cambridge University Press, 2006.

[51] A. Czarnecki and W. J. Marciano, "The Muon anomalous magnetic moment: A Harbinger for 'new physics'," *Phys. Rev. D* **64** (2001) 013014, arXiv:hep-ph/0102122.

[52] J. L. Feng and K. T. Matchev, "Supersymmetry and the anomalous magnetic moment of the muon," *Phys. Rev. Lett.* **86** (2001) 3480–3483, arXiv:hep-ph/0102146.

[53] S. Coleman and J. Mandula, "All possible symmetries of the $s$ matrix," *Phys. Rev.* **159** (Jul, 1967) 1251–1256. https://link.aps.org/doi/10.1103/PhysRev.159.1251.

[54] R. Haag, J. T. Lopuszanski, and M. Sohnius, "All Possible Generators of Supersymmetries of the s Matrix," *Nucl. Phys.* **B88** (1975) 257. [,257(1974)].

[55] J. Wess and B. Zumino, "Supergauge transformations in four dimensions," *Nuclear Physics B* **70** no. 1, (1974) 39 – 50. http://www.sciencedirect.com/science/article/pii/0550321374903551.

[56] H. Georgi and S. L. Glashow, "Gauge theories without anomalies," *Phys. Rev. D* **6** (Jul, 1972) 429–431. https://link.aps.org/doi/10.1103/PhysRevD.6.429.

[57] S. Dimopoulos and D. W. Sutter, "The Supersymmetric flavor problem," *Nucl. Phys. B* **452** (1995) 496–512, arXiv:hep-ph/9504415.

[58] **MEG** Collaboration, T. Mori, "Final Results of the MEG Experiment," *Nuovo Cim. C* **39** no. 4, (2017) 325, arXiv:1606.08168 [hep-ex].

[59] H. P. Nilles, "Supersymmetry, Supergravity and Particle Physics," *Phys. Rept.* **110** (1984) 1–162.

[60] A. Lahanas and D. Nanopoulos, "The road to no-scale supergravity," *Physics Reports* **145** no. 1, (1987) 1 – 139. http://www.sciencedirect.com/science/article/pii/0370157387900342.

[61] J. L. Feng, A. Rajaraman, and F. Takayama, "Superweakly interacting massive particles," *Phys. Rev. Lett.* **91** (2003) 011302, arXiv:hep-ph/0302215.

[62] **Super-Kamiokande** Collaboration, K. Abe *et al.*, "Search for proton decay via $p \to e^+\pi^0$ and $p \to \mu^+\pi^0$ in 0.31 megaton-years exposure of the Super-Kamiokande water Cherenkov detector," *Phys. Rev.* **D95** no. 1, (2017) 012004, arXiv:1610.03597 [hep-ex].

[63] J. R. Ellis, "Beyond the standard model for hill walkers," in *1998 European School of High-Energy Physics*, pp. 133–196. 8, 1998. arXiv:hep-ph/9812235.

[64] J. R. Ellis, J. Hagelin, D. V. Nanopoulos, K. A. Olive, and M. Srednicki, "Supersymmetric Relics from the Big Bang," *Nucl. Phys. B* **238** (1984) 453–476.

[65] D. O. Caldwell, R. M. Eisberg, D. M. Grumm, M. S. Witherell, B. Sadoulet, F. S. Goulding, and A. R. Smith, "Laboratory limits on galactic cold dark matter," *Phys. Rev. Lett.* **61** (Aug, 1988) 510–513. https://link.aps.org/doi/10.1103/PhysRevLett.61.510.

[66] M. Mori, M. M. Nojiri, K. S. Hirata, K. Kihara, Y. Oyama, A. Suzuki, K. Takahashi, M. Yamada, H. Takei, M. Koga, K. Miyano, H. Miyata, Y. Fukuda, T. Hayakawa, K. Inoue, T. Ishida, T. Kajita, Y. Koshio, M. Nakahata, K. Nakamura, A. Sakai, N. Sato, M. Shiozawa, J. Suzuki, Y. Suzuki, Y. Totsuka, M. Koshiba, K. Nishijima, T. Kajimura, T. Suda, A. T. Suzuki, T. Hara, Y. Nagashima, M. Takita, H. Yokoyama, A. Yoshimoto, K. Kaneyuki, Y. Takeuchi, T. Tanimori, S. Tasaka, and K. Nishikawa, "Search for neutralino dark matter heavier than the $w$ boson at kamiokande," *Phys. Rev. D* **48** (Dec, 1993) 5505–5518. https://link.aps.org/doi/10.1103/PhysRevD.48.5505.

[67] **CDMS** Collaboration, D. S. Akerib *et al.*, "Exclusion limits on the WIMP-nucleon cross section from the first run of the Cryogenic Dark Matter Search in the Soudan Underground Laboratory," *Phys. Rev. D* **72** (2005) 052009, arXiv:astro-ph/0507190.

[68] A. Djouadi, J.-L. Kneur, and G. Moultaka, "SuSpect: A Fortran code for the supersymmetric and Higgs particle spectrum in the MSSM," *Comput. Phys. Commun.* **176** (2007) 426–455, arXiv:hep-ph/0211331.

[69] C. F. Berger, J. S. Gainer, J. L. Hewett, and T. G. Rizzo, "Supersymmetry without prejudice," *Journal of High Energy Physics* **2009** no. 02, (Feb, 2009) 023–023. http://dx.doi.org/10.1088/1126-6708/2009/02/023.

[70] J. Alwall, P. Schuster, and N. Toro, "Simplified Models for a First Characterization of New Physics at the LHC," *Phys. Rev.* **D79** (2009) 075020, arXiv:0810.3921 [hep-ph].

[71] **LHC New Physics Working Group** Collaboration, D. Alves, "Simplified Models for LHC New Physics Searches," *J. Phys.* **G39** (2012) 105005, arXiv:1105.2838 [hep-ph].

[72] D. S. Alves, E. Izaguirre, and J. G. Wacker, "Where the Sidewalk Ends: Jets and Missing Energy Search Strategies for the 7 TeV LHC," *JHEP* **10** (2011) 012, arXiv:1102.5338 [hep-ph].

[73] F. Ambrogi, S. Kraml, S. Kulkarni, U. Laa, A. Lessa, and W. Waltenberger, "On the coverage of the pMSSM by simplified model results," *Eur. Phys. J. C* **78** no. 3, (2018) 215, arXiv:1707.09036 [hep-ph].

[74] O. Buchmueller and J. Marrouche, "Universal mass limits on gluino and third-generation squarks in the context of Natural-like SUSY spectra," *Int. J. Mod. Phys. A* **29** no. 06, (2014) 1450032, arXiv:1304.2185 [hep-ph].

[75] **ATLAS** Collaboration, M. Aaboud *et al.*, "Dark matter interpretations of ATLAS searches for the electroweak production of supersymmetric particles in $\sqrt{s} = 8$ TeV proton-proton collisions," *JHEP* **09** (2016) 175, arXiv:1608.00872 [hep-ex].

[76] **ATLAS** Collaboration, "Summary of the ATLAS experiment's sensitivity to supersymmetry after LHC Run 1 — interpreted in the phenomenological MSSM," *JHEP* **10** (2015) 134, arXiv:1508.06608 [hep-ex].

[77] **ATLAS** Collaboration, "Mass reach of the atlas searches for supersymmetry." https://atlas.web.cern.ch/Atlas/GROUPS/PHYSICS/PUBNOTES/ATL-PHYS-PUB-2020-020/fig_23.png, 2020.

[78] **CMS** Collaboration, "Summary plot moriond 2017." https://twiki.cern.ch/twiki/pub/CMSPublic/SUSYSummary2017/Moriond2017_BarPlot.pdf, 2017.

[79] L. S. W. Group, "Notes lepsusywg/02-04.1 and lepsusywg/01-03.1." http://lepsusy.web.cern.ch/lepsusy/, 2004. Accessed: 2021-02-11.

[80] **ATLAS** Collaboration, G. Aad *et al.*, "Observation of a new particle in the search for the Standard Model Higgs boson with the ATLAS detector at the LHC," *Phys. Lett. B* **716** (2012) 1–29, arXiv:1207.7214 [hep-ex].

[81] **CMS** Collaboration, S. Chatrchyan *et al.*, "Observation of a New Boson at a Mass of 125 GeV with the CMS Experiment at the LHC," *Phys. Lett. B* **716** (2012) 30–61, arXiv:1207.7235 [hep-ex].

[82] CERN, "About cern." https://home.cern/about. Accessed: 2021-01-21.

[83] CERN, "CERN Annual report 2019," tech. rep., CERN, Geneva, 2020. https://cds.cern.ch/record/2723123.

[84] O. S. Bruning, P. Collier, P. Lebrun, S. Myers, R. Ostojic, J. Poole, and P. Proudlock, *LHC Design Report*. CERN Yellow Reports: Monographs. CERN, Geneva, 2004. https://cds.cern.ch/record/782076.

[85] M. Blewett and N. Vogt-Nilsen, "Proceedings of the 8th international conference on high-energy accelerators, cern 1971. conference held at geneva, 20–24 september 1971.," tech. rep., 1971, 1971.

[86] L. R. Evans and P. Bryant, "LHC Machine," *JINST* **3** (2008) S08001. 164 p. http://cds.cern.ch/record/1129806. This report is an abridged version of the LHC Design Report (CERN-2004-003).

[87] R. Scrivens, M. Kronberger, D. Küchler, J. Lettry, C. Mastrostefano, O. Midttun, M. O'Neil, H. Pereira, and C. Schmitzer, "Overview of the status and developments on primary ion sources at CERN*,". https://cds.cern.ch/record/1382102.

[88] M. Vretenar, J. Vollaire, R. Scrivens, C. Rossi, F. Roncarolo, S. Ramberger, U. Raich, B. Puccio, D. Nisbet, R. Mompo, S. Mathot, C. Martin, L. A. Lopez-Hernandez, A. Lombardi, J. Lettry, J. B. Lallement, I. Kozsar, J. Hansen, F. Gerigk, A. Funken, J. F. Fuchs, N. Dos Santos, M. Calviani, M. Buzio, O. Brunner, Y. Body, P. Baudrenghien, J. Bauche, and T. Zickler, *Linac4 design report*, vol. 6 of *CERN Yellow Reports: Monographs*. CERN, Geneva, 2020. https://cds.cern.ch/record/2736208.

[89] E. Mobs, "The CERN accelerator complex - 2019. Complexe des accélérateurs du CERN - 2019,". https://cds.cern.ch/record/2684277. General Photo.

[90] **ATLAS** Collaboration, "The ATLAS Experiment at the CERN Large Hadron Collider," *JINST* **3** (2008) S08003.

[91] **CMS** Collaboration, S. Chatrchyan *et al.*, "The CMS Experiment at the CERN LHC," *JINST* **3** (2008) S08004.

[92] **ALICE** Collaboration, K. Aamodt *et al.*, "The ALICE experiment at the CERN LHC," *JINST* **3** (2008) S08002.

[93] **LHCb** Collaboration, J. Alves, A.Augusto *et al.*, "The LHCb Detector at the LHC," *JINST* **3** (2008) S08005.

[94] **TOTEM** Collaboration, G. Anelli *et al.*, "The TOTEM experiment at the CERN Large Hadron Collider," *JINST* **3** (2008) S08007.

[95] **LHCf** Collaboration, O. Adriani *et al.*, "Technical design report of the LHCf experiment: Measurement of photons and neutral pions in the very forward region of LHC,".

[96] **MoEDAL** Collaboration, J. Pinfold *et al.*, "Technical Design Report of the MoEDAL Experiment,".

[97] **ATLAS** Collaboration, "ATLAS Public Results - Luminosity Public Results Run 2,". https://twiki.cern.ch/twiki/bin/view/AtlasPublic/LuminosityPublicResultsRun2. Accessed: 2021-01-17.

[98] **ATLAS** Collaboration, Z. Marshall, "Simulation of Pile-up in the ATLAS Experiment," *J. Phys. Conf. Ser.* **513** (2014) 022024.

[99] "First beam in the LHC - accelerating science,". https://home.cern/news/news/accelerators/record-luminosity-well-done-lhc. Accessed: 2021-01-10.

[100] **ATLAS Collaboration** Collaboration, "Luminosity determination in $pp$ collisions at $\sqrt{s} = 13$ TeV using the ATLAS detector at the LHC," Tech. Rep. ATLAS-CONF-2019-021, CERN, Geneva, Jun, 2019. https://cds.cern.ch/record/2677054.

[101] **ATLAS** Collaboration, M. Aaboud *et al.*, "Luminosity determination in pp collisions at $\sqrt{s} = 8$ TeV using the ATLAS detector at the LHC," *Eur. Phys. J. C* **76** no. 12, (2016) 653, arXiv:1608.03953 [hep-ex].

[102] G. Avoni, M. Bruschi, G. Cabras, D. Caforio, N. Dehghanian, A. Floderus, B. Giacobbe, F. Giannuzzi, F. Giorgi, P. Grafström, V. Hedberg, F. L. Manghi, S. Meneghini, J. Pinfold, E. Richards, C. Sbarra, N. S. Cesari, A. Sbrizzi, R. Soluk, G. Ucchielli, S. Valentinetti, O. Viazlo, M. Villa, C. Vittori, R. Vuillermet, and A. Zoccoli, "The new LUCID-2 detector for luminosity measurement and monitoring in ATLAS," *Journal of Instrumentation* **13** no. 07, (Jul, 2018) P07017–P07017. https://doi.org/10.1088/1748-0221/13/07/p07017.

[103] S. van der Meer, "Calibration of the effective beam height in the ISR," Tech. Rep. CERN-ISR-PO-68-31. ISR-PO-68-31, CERN, Geneva, 1968. https://cds.cern.ch/record/296752.

[104] P. Grafström and W. Kozanecki, "Luminosity determination at proton colliders," *Progress in Particle and Nuclear Physics* **81** (2015) 97 – 148. http://www.sciencedirect.com/science/article/pii/S0146641014000878.

[105] "New schedule for CERN's accelerators and experiments,". https://home.cern/news/press-release/cern/first-beam-lhc-accelerating-science. Accessed: 2021-01-10.

[106] **ATLAS** Collaboration, G. Aad *et al.*, "Luminosity Determination in *pp* Collisions at $\sqrt{s} = 7$ TeV Using the ATLAS Detector at the LHC," *Eur. Phys. J. C* **71** (2011) 1630, arXiv:1101.2185 [hep-ex].

[107] **ATLAS Collaboration** Collaboration, G. Aad *et al.*, "Improved luminosity determination in pp collisions at $\sqrt{s} = 7$ TeV using the ATLAS detector at the LHC. Improved luminosity determination in pp collisions at sqrt(s) = 7 TeV using the ATLAS detector at the LHC," *Eur. Phys. J. C* **73** no. CERN-PH-EP-2013-026. CERN-PH-EP-2013-026, (Feb, 2013) 2518. 27 p. https://cds.cern.ch/record/1517411. Comments: 26 pages plus author list (39 pages total), 17 figures, 9 tables, submitted to EPJC, All figures are available at <a href=.

[108] "Record luminosity: well done LHC,". https://home.cern/news/news/accelerators/new-schedule-cerns-accelerators-and-experiments. Accessed: 2021-01-10.

[109] A. G., B. A. I., B. O., F. P., L. M., R. L., and T. L., *High-Luminosity Large Hadron Collider (HL-LHC): Technical Design Report V. 0.1*. CERN Yellow Reports: Monographs. CERN, Geneva, 2017. https://cds.cern.ch/record/2284929.

[110] J. Pequenao, "Computer generated image of the whole ATLAS detector." Mar, 2008.

[111] **ATLAS** Collaboration, "ATLAS: Detector and physics performance technical design report. Volume 1,".

[112] J. Pequenao, "Computer generated image of the ATLAS inner detector." Mar, 2008.

[113] **ATLAS Collaboration** Collaboration, K. Potamianos, "The upgraded Pixel detector and the commissioning of the Inner Detector tracking of the ATLAS experiment for Run-2 at the Large Hadron Collider," Tech. Rep. ATL-PHYS-PROC-2016-104, CERN, Geneva, Aug, 2016. https://cds.cern.ch/record/2209070. 15 pages, EPS-HEP 2015 Proceedings.

[114] **ATLAS IBL** Collaboration, B. Abbott *et al.*, "Production and Integration of the ATLAS Insertable B-Layer," *JINST* **13** no. 05, (2018) T05008, arXiv:1803.00844 [physics.ins-det].

[115] **ATLAS** Collaboration, "ATLAS Insertable B-Layer Technical Design Report," Tech. Rep. CERN-LHCC-2010-013. ATLAS-TDR-19, Sep, 2010. http://cds.cern.ch/record/1291633.

[116] **ATLAS** Collaboration, G. Aad *et al.*, "ATLAS b-jet identification performance and efficiency measurement with $t\bar{t}$ events in pp collisions at $\sqrt{s} = 13$ TeV," *Eur. Phys. J. C* **79** no. 11, (2019) 970, arXiv:1907.05120 [hep-ex].

[117] ATLAS Collaboration, "Particle Identification Performance of the ATLAS Transition Radiation Tracker." ATLAS-CONF-2011-128, 2011. https://cds.cern.ch/record/1383793.

[118] J. Pequenao, "Computer Generated image of the ATLAS calorimeter." Mar, 2008.

[119] J. Pequenao, "Computer generated image of the ATLAS Muons subsystem." Mar, 2008.

[120] S. Lee, M. Livan, and R. Wigmans, "Dual-Readout Calorimetry," *Rev. Mod. Phys.* **90** no. arXiv:1712.05494. 2, (Dec, 2017) 025002. 40 p. https://cds.cern.ch/record/2637852. 44 pages, 53 figures, accepted for publication in Review of Modern Physics.

[121] M. Leite, "Performance of the ATLAS Zero Degree Calorimeter," Tech. Rep. ATL-FWD-PROC-2013-001, CERN, Geneva, Nov, 2013. https://cds.cern.ch/record/1628749.

[122] S. Abdel Khalek *et al.*, "The ALFA Roman Pot Detectors of ATLAS," *JINST* **11** no. 11, (2016) P11013, arXiv:1609.00249 [physics.ins-det].

[123] U. Amaldi, G. Cocconi, A. Diddens, R. Dobinson, J. Dorenbosch, W. Duinker, D. Gustavson, J. Meyer, K. Potter, A. Wetherell, A. Baroncelli, and C. Bosio, "The real part of the forward proton proton scattering amplitude measured at the cern intersecting storage rings," *Physics Letters B* **66** no. 4, (1977) 390 – 394. http://www.sciencedirect.com/science/article/pii/0370269377900223.

[124] L. Adamczyk, E. Banaś, A. Brandt, M. Bruschi, S. Grinstein, J. Lange, M. Rijssenbeek, P. Sicho, R. Staszewski, T. Sykora, M. Trzebiński, J. Chwastowski, and K. Korcyl, "Technical Design Report for the ATLAS Forward Proton Detector," Tech. Rep. CERN-LHCC-2015-009. ATLAS-TDR-024, May, 2015. https://cds.cern.ch/record/2017378.

[125] **ATLAS** Collaboration, A. R. Martínez, "The Run-2 ATLAS Trigger System," *J. Phys. Conf. Ser.* **762** no. 1, (2016) 012003.

[126] **ATLAS Collaboration** Collaboration, *ATLAS level-1 trigger: Technical Design Report*. Technical Design Report ATLAS. CERN, Geneva, 1998. https://cds.cern.ch/record/381429.

[127] **ATLAS** Collaboration, G. Aad *et al.*, "Operation of the ATLAS trigger system in Run 2," *JINST* **15** no. 10, (2020) P10004, arXiv:2007.12539 [physics.ins-det].

[128] **ATLAS Collaboration** Collaboration, P. Jenni, M. Nessi, M. Nordberg, and K. Smith, *ATLAS high-level trigger, data-acquisition and controls: Technical Design Report*. Technical Design Report ATLAS. CERN, Geneva, 2003. https://cds.cern.ch/record/616089.

[129] **ATLAS** Collaboration, G. Aad *et al.*, "The ATLAS Simulation Infrastructure," *Eur. Phys. J. C* **70** (2010) 823–874, arXiv:1005.4568 [physics.ins-det].

[130] T. Gleisberg, S. Hoeche, F. Krauss, M. Schonherr, S. Schumann, F. Siegert, and J. Winter, "Event generation with SHERPA 1.1," *JHEP* **02** (2009) 007, arXiv:0811.4622 [hep-ph].

[131] A. Buckley *et al.*, "General-purpose event generators for LHC physics," *Phys. Rept.* **504** (2011) 145–233, arXiv:1101.2599 [hep-ph].

[132] V. N. Gribov and L. N. Lipatov, "Deep inelastic e p scattering in perturbation theory," *Sov. J. Nucl. Phys.* **15** (1972) 438–450.

[133] J. Blumlein, T. Doyle, F. Hautmann, M. Klein, and A. Vogt, "Structure functions in deep inelastic scattering at HERA," in *Workshop on Future Physics at HERA (To be followed by meetings 7-9 Feb and 30-31 May 1996 at DESY)*. 9, 1996. arXiv:hep-ph/9609425.

[134] A. Buckley, J. Ferrando, S. Lloyd, K. Nordström, B. Page, M. Rüfenacht, M. Schönherr, and G. Watt, "LHAPDF6: parton density access in the LHC precision era," *Eur. Phys. J. C* **75** (2015) 132, arXiv:1412.7420 [hep-ph].

[135] M. Bengtsson and T. Sjostrand, "Coherent Parton Showers Versus Matrix Elements: Implications of PETRA - PEP Data," *Phys. Lett. B* **185** (1987) 435.

[136] S. Catani, F. Krauss, R. Kuhn, and B. R. Webber, "QCD matrix elements + parton showers," *JHEP* **11** (2001) 063, arXiv:hep-ph/0109231.

[137] L. Lonnblad, "Correcting the color dipole cascade model with fixed order matrix elements," *JHEP* **05** (2002) 046, arXiv:hep-ph/0112284.

[138] B. Andersson, G. Gustafson, G. Ingelman, and T. Sjostrand, "Parton Fragmentation and String Dynamics," *Phys. Rept.* **97** (1983) 31–145.

[139] B. Andersson, *The Lund Model*. Cambridge Monographs on Particle Physics, Nuclear Physics and Cosmology. Cambridge University Press, 1998.

[140] D. Amati and G. Veneziano, "Preconfinement as a Property of Perturbative QCD," *Phys. Lett. B* **83** (1979) 87–92.

[141] D. Yennie, S. Frautschi, and H. Suura, "The infrared divergence phenomena and high-energy processes," *Annals of Physics* **13** no. 3, (1961) 379–452. https://www.sciencedirect.com/science/article/pii/0003491661901518.

[142] M. Dobbs and J. B. Hansen, "The HepMC C++ Monte Carlo event record for High Energy Physics," *Comput. Phys. Commun.* **134** (2001) 41–46.

[143] **GEANT4** Collaboration, S. Agostinelli *et al.*, "GEANT4: A Simulation toolkit," *Nucl. Instrum. Meth.* **A506** (2003) 250–303.

[144] **ATLAS Collaboration** Collaboration, "The new Fast Calorimeter Simulation in ATLAS," Tech. Rep. ATL-SOFT-PUB-2018-002, CERN, Geneva, Jul, 2018. https://cds.cern.ch/record/2630434.

[145] K. Cranmer, "Practical Statistics for the LHC," in *2011 European School of High-Energy Physics*, pp. 267–308. 2014. arXiv:1503.07622 [physics.data-an].

[146] G. Cowan, K. Cranmer, E. Gross, and O. Vitells, "Asymptotic formulae for likelihood-based tests of new physics," *Eur. Phys. J.* **C71** (2011) 1554, arXiv:1007.1727 [physics.data-an]. [Erratum: Eur. Phys. J.C73,2501(2013)].

[147] ATLAS Collaboration, "Reproduction searches for new physics with the ATLAS experiment through publication of full statistical likelihoods." ATL-PHYS-PUB-2019-029, 2019. https://cds.cern.ch/record/2684863.

[148] **ROOT Collaboration** Collaboration, K. Cranmer, G. Lewis, L. Moneta, A. Shibata, and W. Verkerke, "HistFactory: A tool for creating statistical models for use with RooFit and RooStats," Tech. Rep. CERN-OPEN-2012-016, New York U., New York, Jan, 2012. https://cds.cern.ch/record/1456844.

[149] W. Verkerke and D. P. Kirkby, "The RooFit toolkit for data modeling," *eConf* **C0303241** (2003) MOLT007, arXiv:physics/0306116 [physics]. [,186(2003)].

[150] L. Moneta, K. Belasco, K. S. Cranmer, S. Kreiss, A. Lazzaro, D. Piparo, G. Schott, W. Verkerke, and M. Wolf, "The RooStats Project," *PoS* **ACAT2010** (2010) 057, arXiv:1009.1003 [physics.data-an].

[151] F. James and M. Roos, "MINUIT: a system for function minimization and analysis of the parameter errors and corrections," *Comput. Phys. Commun.* **10** no. CERN-DD-75-20, (Jul, 1975) 343–367. 38 p. https://cds.cern.ch/record/310399.

[152] R. Brun and F. Rademakers, "ROOT: An object oriented data analysis framework," *Nucl. Instrum. Meth.* **A389** (1997) 81–86.

[153] I. Antcheva *et al.*, "Root — a c++ framework for petabyte data storage, statistical analysis and visualization," *Computer Physics Communications* **182** no. 6, (2011) 1384 – 1385. http://www.sciencedirect.com/science/article/pii/S0010465511000701.

[154] M. Baak, G. J. Besjes, D. Côte, A. Koutsman, J. Lorenz, and D. Short, "HistFitter software framework for statistical data analysis," *Eur. Phys. J.* **C75** (2015) 153, `arXiv:1410.1280 [hep-ex]`.

[155] L. Heinrich, M. Feickert, G. Stark, and K. Cranmer, "pyhf: pure-python implementation of histfactory statistical models," *Journal of Open Source Software* **6** no. 58, (2021) 2823. https://doi.org/10.21105/joss.02823.

[156] L. Heinrich, M. Feickert, and G. Stark, "pyhf: v0.6.0." https://github.com/scikit-hep/pyhf.

[157] C. R. Harris, K. J. Millman, S. J. van der Walt, R. Gommers, P. Virtanen, D. Cournapeau, E. Wieser, J. Taylor, S. Berg, N. J. Smith, R. Kern, M. Picus, S. Hoyer, M. H. van Kerkwijk, M. Brett, A. Haldane, J. F. del R'ıo, M. Wiebe, P. Peterson, P. G'erard-Marchant, K. Sheppard, T. Reddy, W. Weckesser, H. Abbasi, C. Gohlke, and T. E. Oliphant, "Array programming with NumPy," *Nature* **585** no. 7825, (Sept., 2020) 357–362. https://doi.org/10.1038/s41586-020-2649-2.

[158] A. Paszke, S. Gross, F. Massa, A. Lerer, J. Bradbury, G. Chanan, T. Killeen, Z. Lin, N. Gimelshein, L. Antiga, A. Desmaison, A. Kopf, E. Yang, Z. DeVito, M. Raison, A. Tejani, S. Chilamkurthy, B. Steiner, L. Fang, J. Bai, and S. Chintala, "Pytorch: An imperative style, high-performance deep learning library," in *Advances in Neural Information Processing Systems 32*, H. Wallach, H. Larochelle, A. Beygelzimer, F. d'Alché-Buc, E. Fox, and R. Garnett, eds., pp. 8024–8035. Curran Associates, Inc., 2019. http://papers.neurips.cc/paper/9015-pytorch-an-imperative-style-high-performance-deep-learning-library.pdf.

[159] M. Abadi, A. Agarwal, P. Barham, E. Brevdo, Z. Chen, C. Citro, G. S. Corrado, A. Davis, J. Dean, M. Devin, S. Ghemawat, I. Goodfellow, A. Harp, G. Irving, M. Isard, Y. Jia, R. Jozefowicz, L. Kaiser, M. Kudlur, J. Levenberg, D. Mané, R. Monga, S. Moore, D. Murray, C. Olah, M. Schuster, J. Shlens, B. Steiner, I. Sutskever, K. Talwar, P. Tucker, V. Vanhoucke, V. Vasudevan, F. Viégas, O. Vinyals, P. Warden, M. Wattenberg, M. Wicke, Y. Yu, and X. Zheng, "TensorFlow: Large-scale machine learning on heterogeneous systems," 2015. https://www.tensorflow.org/. Software available from tensorflow.org.

[160] J. Bradbury, R. Frostig, P. Hawkins, M. J. Johnson, C. Leary, D. Maclaurin, and S. Wanderman-Milne, "JAX: composable transformations of Python+NumPy programs," 2018. http://github.com/google/jax.

[161] S. S. Wilks, "The large-sample distribution of the likelihood ratio for testing composite hypotheses," *Ann. Math. Statist.* **9** no. 1, (03, 1938) 60–62. https://doi.org/10.1214/aoms/1177732360.

[162] A. Wald, "Tests of statistical hypotheses concerning several parameters when the number of observations is large," *Transactions of the American Mathematical Society* **54** no. 3, (1943) 426–482. https://doi.org/10.1090/S0002-9947-1943-0012401-3.

[163] G. Cowan, "Statistics for Searches at the LHC," in *69th Scottish Universities Summer School in Physics: LHC Physics*, pp. 321–355. 7, 2013. arXiv:1307.2487 [hep-ex].

[164] A. L. Read, "Presentation of search results: the $CL_S$ technique," *J. Phys. G* **28** (2002) 2693.

[165] R. D. Cousins, J. T. Linnemann, and J. Tucker, "Evaluation of three methods for calculating statistical significance when incorporating a systematic uncertainty into a test of the background-only hypothesis for a Poisson process," *Nucl. Instrum. Meth. A* **595** no. 2, (2008) 480, arXiv:physics/0702156 [physics.data-an].

[166] K. CRANMER, "Statistical challenges for searches for new physics at the lhc," *Statistical Problems in Particle Physics, Astrophysics and Cosmology* (May, 2006) . http://dx.doi.org/10.1142/9781860948985_0026.

[167] ATLAS Collaboration, "Search for direct pair production of a chargino and a neutralino decaying to the 125 GeV Higgs boson in $\sqrt{s} = 8$ TeV $pp$ collisions with the ATLAS detector," *Eur. Phys. J. C* **75** (2015) 208, arXiv:1501.07110 [hep-ex].

[168] ATLAS Collaboration, "Search for chargino and neutralino production in final states with a Higgs boson and missing transverse momentum at $\sqrt{s} = 13$ TeV with the ATLAS detector," *Phys. Rev. D* **100** (2019) 012006, arXiv:1812.09432 [hep-ex].

[169] CMS Collaboration, "Search for electroweak production of charginos and neutralinos in $WH$ events in proton–proton collisions at $\sqrt{s} = 13$ TeV," *JHEP* **11** (2017) 029, arXiv:1706.09933 [hep-ex].

[170] ATLAS Collaboration, "Search for direct production of electroweakinos in final states with one lepton, missing transverse momentum and a Higgs boson decaying into two $b$-jets in $pp$ collisions at $\sqrt{s} = 13$ TeV with the ATLAS detector," *Eur. Phys. J. C* **80** (2020) 691, arXiv:1909.09226 [hep-ex].

[171] ATLAS Collaboration, "Improvements in $t\bar{t}$ modelling using NLO+PS Monte Carlo generators for Run 2." ATL-PHYS-PUB-2018-009, 2018. https://cds.cern.ch/record/2630327.

[172] ATLAS Collaboration, "Modelling of the $t\bar{t}H$ and $t\bar{t}V(V = W, Z)$ processes for $\sqrt{s} = 13$ TeV ATLAS analyses." ATL-PHYS-PUB-2016-005, 2016. https://cds.cern.ch/record/2120826.

[173] ATLAS Collaboration, "ATLAS simulation of boson plus jets processes in Run 2." ATL-PHYS-PUB-2017-006, 2017. https://cds.cern.ch/record/2261937.

[174] ATLAS Collaboration, "Multi-Boson Simulation for 13 TeV ATLAS Analyses." ATL-PHYS-PUB-2017-005, 2017. https://cds.cern.ch/record/2261933.

[175] J. Alwall, R. Frederix, S. Frixione, V. Hirschi, F. Maltoni, O. Mattelaer, H. S. Shao, T. Stelzer, P. Torrielli, and M. Zaro, "The automated computation of tree-level and next-to-leading order differential cross sections, and their matching to parton shower simulations," *JHEP* **07** (2014) 079, arXiv:1405.0301 [hep-ph].

[176] R. Frederix and S. Frixione, "Merging meets matching in MC@NLO," *JHEP* **12** (2012) 061, arXiv:1209.6215 [hep-ph].

[177] T. Sjöstrand, S. Ask, J. R. Christiansen, R. Corke, N. Desai, P. Ilten, S. Mrenna, S. Prestel, C. O. Rasmussen, and P. Z. Skands, "An Introduction to PYTHIA 8.2," *Comput. Phys. Commun.* **191** (2015) 159–177, arXiv:1410.3012 [hep-ph].

[178] L. Lönnblad and S. Prestel, "Matching tree-level matrix elements with interleaved showers," *JHEP* **03** (2012) 019, arXiv:1109.4829 [hep-ph].

[179] R. D. Ball *et al.*, "Parton distributions with LHC data," *Nucl. Phys. B* **867** (2013) 244, arXiv:1207.1303 [hep-ph].

[180] ATLAS Collaboration, "ATLAS Pythia 8 tunes to 7 TeV data." ATL-PHYS-PUB-2014-021, 2014. https://cds.cern.ch/record/1966419.

[181] D. J. Lange, "The EvtGen particle decay simulation package," *Nucl. Instrum. Meth. A* **462** (2001) 152.

[182] ATLAS Collaboration, "The Pythia 8 A3 tune description of ATLAS minimum bias and inelastic measurements incorporating the Donnachie–Landshoff diffractive model." ATL-PHYS-PUB-2016-017, 2016. https://cds.cern.ch/record/2206965.

[183] B. Fuks, M. Klasen, D. R. Lamprea, and M. Rothering, "Precision predictions for electroweak superpartner production at hadron colliders with RESUMMINO," *Eur. Phys. J. C* **73** (2013) 2480, arXiv:1304.0790 [hep-ph].

[184] J. Fiaschi and M. Klasen, "Neutralino-chargino pair production at NLO+NLL with resummation-improved parton density functions for LHC Run II," *Phys. Rev. D* **98** no. 5, (2018) 055014, arXiv:1805.11322 [hep-ph].

[185] B. Fuks, M. Klasen, D. R. Lamprea, and M. Rothering, "Gaugino production in proton-proton collisions at a center-of-mass energy of 8 TeV," *JHEP* **10** (2012) 081, arXiv:1207.2159 [hep-ph].

[186] S. Alioli, P. Nason, C. Oleari, and E. Re, "A general framework for implementing NLO calculations in shower Monte Carlo programs: the POWHEG BOX," *JHEP* **06** (2010) 043, arXiv:1002.2581 [hep-ph].

[187] S. Frixione, P. Nason, and G. Ridolfi, "A Positive-weight next-to-leading-order Monte Carlo for heavy flavour hadroproduction," *JHEP* **09** (2007) 126, arXiv:0707.3088 [hep-ph].

[188] P. Nason, "A New method for combining NLO QCD with shower Monte Carlo algorithms," *JHEP* **11** (2004) 040, arXiv:hep-ph/0409146.

[189] E. Bothmann *et al.*, "Event generation with Sherpa 2.2," *SciPost Phys.* **7** no. 3, (2019) 034, arXiv:1905.09127 [hep-ph].

[190] S. Höche, F. Krauss, S. Schumann, and F. Siegert, "QCD matrix elements and truncated showers," *JHEP* **05** (2009) 053, arXiv:0903.1219 [hep-ph].

[191] S. Höche, F. Krauss, M. Schönherr, and F. Siegert, "QCD matrix elements + parton showers. The NLO case," *JHEP* **04** (2013) 027, arXiv:1207.5030 [hep-ph].

[192] **NNPDF** Collaboration, R. D. Ball *et al.*, "Parton distributions for the LHC run II," *JHEP* **04** (2015) 040, arXiv:1410.8849 [hep-ph].

[193] ATLAS Collaboration, "Example ATLAS tunes of Pythia8, Pythia6 and Powheg to an observable sensitive to $Z$ boson transverse momentum." ATL-PHYS-PUB-2013-017, 2013. https://cds.cern.ch/record/1629317.

[194] M. Czakon and A. Mitov, "Top++: A program for the calculation of the top-pair cross-section at hadron colliders," *Comput. Phys. Commun.* **185** (2014) 2930, arXiv:1112.5675 [hep-ph].

[195] M. Cacciari, M. Czakon, M. Mangano, A. Mitov, and P. Nason, "Top-pair production at hadron colliders with next-to-next-to-leading logarithmic soft-gluon resummation," *Phys. Lett. B* **710** (2012) 612–622, arXiv:1111.5869 [hep-ph].

[196] P. Kant, O. M. Kind, T. Kintscher, T. Lohse, T. Martini, S. Mölbitz, P. Rieck, and P. Uwer, "HatHor for single top-quark production: Updated predictions and uncertainty estimates for single top-quark production in hadronic collisions," *Comput. Phys. Commun.* **191** (2015) 74–89, arXiv:1406.4403 [hep-ph].

[197] N. Kidonakis, "Two-loop soft anomalous dimensions for single top quark associated production with a $W^-$ or $H^-$," *Phys. Rev. D* **82** (2010) 054018, arXiv:1005.4451 [hep-ph].

[198] J. M. Campbell and R. K. Ellis, "$t\bar{t}W^{+-}$ production and decay at NLO," *JHEP* **07** (2012) 052, arXiv:1204.5678 [hep-ph].

[199] A. Lazopoulos, T. McElmurry, K. Melnikov, and F. Petriello, "Next-to-leading order QCD corrections to $t\bar{t}Z$ production at the LHC," *Phys. Lett. B* **666** (2008) 62–65, arXiv:0804.2220 [hep-ph].

[200] R. Gavin, Y. Li, F. Petriello, and S. Quackenbush, "FEWZ 2.0: A code for hadronic $Z$ production at next-to-next-to-leading order," arXiv:1011.3540 [hep-ph].

[201] **LHC Higgs Cross Section Working Group** Collaboration, D. de Florian *et al.*, "Handbook of LHC Higgs Cross Sections: 4. Deciphering the Nature of the Higgs Sector," arXiv:1610.07922 [hep-ph].

[202] ATLAS Collaboration, "Performance of the ATLAS track reconstruction algorithms in dense environments in LHC Run 2," *Eur. Phys. J. C* **77** (2017) 673, arXiv:1704.07983 [hep-ex].

[203] R. Frühwirth, "Application of Kalman filtering to track and vertex fitting," *Nucl. Instrum. Methods Phys. Res., A* **262** no. HEPHY-PUB-503, (Jun, 1987) 444. 19 p. https://cds.cern.ch/record/178627.

[204] T. Cornelissen, M. Elsing, I. Gavrilenko, W. Liebig, E. Moyse, and A. Salzburger, "The new ATLAS track reconstruction (NEWT)," *J. Phys.: Conf. Ser.* **119** (2008) 032014. https://cds.cern.ch/record/1176900.

[205] ATLAS Collaboration, "Vertex Reconstruction Performance of the ATLAS Detector at $\sqrt{s} = 13$ TeV." ATL-PHYS-PUB-2015-026, 2015. https://cds.cern.ch/record/2037717.

[206] ATLAS Collaboration, "Reconstruction of primary vertices at the ATLAS experiment in Run 1 proton–proton collisions at the LHC," *Eur. Phys. J. C* **77** (2017) 332, arXiv:1611.10235 [hep-ex].

[207] ATLAS Collaboration, "Topological cell clustering in the ATLAS calorimeters and its performance in LHC Run 1," *Eur. Phys. J. C* **77** (2017) 490, arXiv:1603.02934 [hep-ex].

[208] ATLAS Collaboration, "Electron and photon performance measurements with the ATLAS detector using the 2015–2017 LHC proton–proton collision data," *JINST* **14** (2019) P12006, arXiv:1908.00005 [hep-ex].

[209] ATLAS Collaboration, "Measurement of the photon identification efficiencies with the ATLAS detector using LHC Run 2 data collected in 2015 and 2016," *Eur. Phys. J. C* **79** (2019) 205, arXiv:1810.05087 [hep-ex].

[210] ATLAS Collaboration, "Electron reconstruction and identification in the ATLAS experiment using the 2015 and 2016 LHC proton–proton collision data at $\sqrt{s} = 13$ TeV," *Eur. Phys. J. C* **79** (2019) 639, arXiv:1902.04655 [hep-ex].

[211] ATLAS Collaboration, "Muon reconstruction performance of the ATLAS detector in proton–proton collision data at $\sqrt{s} = 13$ TeV," *Eur. Phys. J. C* **76** (2016) 292, arXiv:1603.05598 [hep-ex].

[212] **ATLAS** Collaboration, "Muon reconstruction and identification efficiency in ATLAS using the full Run 2 *pp* collision data set at $\sqrt{s} = 13$ TeV," arXiv:2012.00578 [hep-ex].

[213] M. Cacciari, G. P. Salam, and G. Soyez, "The anti-$k_t$ jet clustering algorithm," *JHEP* **04** (2008) 063, arXiv:0802.1189 [hep-ph].

[214] M. Cacciari, G. P. Salam, and G. Soyez, "FastJet user manual," *Eur. Phys. J. C* **72** (2012) 1896, arXiv:1111.6097 [hep-ph].

[215] M. Cacciari, "FastJet: A Code for fast $k_t$ clustering, and more," in *Deep inelastic scattering. Proceedings, 14th International Workshop, DIS 2006, Tsukuba, Japan, April 20-24, 2006*, pp. 487–490. 2006. arXiv:hep-ph/0607071 [hep-ph]. [,125(2006)].

[216] **ATLAS** Collaboration, G. Aad *et al.*, "Jet energy scale and resolution measured in proton-proton collisions at $\sqrt{s} = 13$ TeV with the ATLAS detector," arXiv:2007.02645 [hep-ex].

[217] M. Cacciari and G. P. Salam, "Pileup subtraction using jet areas," *Phys. Lett. B* **659** (2008) 119–126, arXiv:0707.1378 [hep-ph].

[218] ATLAS Collaboration, "Jet energy measurement with the ATLAS detector in proton–proton collisions at $\sqrt{s} = 7$ TeV," *Eur. Phys. J. C* **73** (2013) 2304, arXiv:1112.6426 [hep-ex].

[219] ATLAS Collaboration, "Determination of jet calibration and energy resolution in proton–proton collisions at $\sqrt{s} = 8$ TeV using the ATLAS detector," arXiv:1910.04482 [hep-ex].

[220] ATLAS Collaboration, "Performance of pile-up mitigation techniques for jets in *pp* collisions at $\sqrt{s} = 8$ TeV using the ATLAS detector," *Eur. Phys. J. C* **76** (2016) 581, arXiv:1510.03823 [hep-ex].

[221] ATLAS Collaboration, "Optimisation and performance studies of the ATLAS *b*-tagging algorithms for the 2017-18 LHC run." ATL-PHYS-PUB-2017-013, 2017. https://cds.cern.ch/record/2273281.

[222] ATLAS Collaboration, "ATLAS $b$-jet identification performance and efficiency measurement with $t\bar{t}$ events in $pp$ collisions at $\sqrt{s} = 13\,\text{TeV}$," *Eur. Phys. J. C* **79** (2019) 970, arXiv:1907.05120 [hep-ex].

[223] ATLAS Collaboration, "Measurements of $b$-jet tagging efficiency with the ATLAS detector using $t\bar{t}$ events at $\sqrt{s} = 13\,\text{TeV}$," *JHEP* **08** (2018) 089, arXiv:1805.01845 [hep-ex].

[224] ATLAS Collaboration, "Performance of missing transverse momentum reconstruction with the ATLAS detector using proton–proton collisions at $\sqrt{s} = 13\,\text{TeV}$," *Eur. Phys. J. C* **78** (2018) 903, arXiv:1802.08168 [hep-ex].

[225] **ATLAS Collaboration** Collaboration, "$E_{\text{T}}^{\text{miss}}$ performance in the ATLAS detector using 2015-2016 LHC p-p collisions," Tech. Rep. ATLAS-CONF-2018-023, CERN, Geneva, Jun, 2018. http://cds.cern.ch/record/2625233.

[226] D. Adams *et al.*, "Recommendations of the Physics Objects and Analysis Harmonisation Study Groups 2014," Tech. Rep. ATL-PHYS-INT-2014-018, CERN, Geneva, Jul, 2014. https://cds.cern.ch/record/1743654.

[227] M. Cacciari, G. P. Salam, and G. Soyez, "The Catchment Area of Jets," *JHEP* **04** (2008) 005, arXiv:0802.1188 [hep-ph].

[228] **UA1** Collaboration, G. Arnison *et al.*, "Experimental Observation of Isolated Large Transverse Energy Electrons with Associated Missing Energy at $\sqrt{s} = 540$ GeV," *Phys. Lett. B* **122** (1983) 103–116.

[229] **Aachen-Annecy-Birmingham-CERN-Helsinki-London(QMC)-Paris(CdF)-Riverside-Rome-Rutherford-Saclay(CEN)-Vienna** Collaboration, G. Arnison *et al.*, "Further evidence for charged intermediate vector bosons at the SPS collider," *Phys. Lett. B* **129** no. CERN-EP-83-111, (Jun, 1985) 273–282. 17 p. https://cds.cern.ch/record/163856.

[230] D. R. Tovey, "On measuring the masses of pair-produced semi-invisibly decaying particles at hadron colliders," *JHEP* **04** (2008) 034, arXiv:0802.2879 [hep-ph].

[231] G. Polesello and D. R. Tovey, "Supersymmetric particle mass measurement with the boost-corrected contransverse mass," *JHEP* **03** (2010) 030, arXiv:0910.0174 [hep-ph].

[232] **ATLAS** Collaboration, G. Aad *et al.*, "Performance of the missing transverse momentum triggers for the ATLAS detector during Run-2 data taking," *JHEP* **08** (2020) 080, arXiv:2005.09554 [hep-ex].

[233] **ATLAS** Collaboration, G. Aad *et al.*, "Performance of algorithms that reconstruct missing transverse momentum in $\sqrt{s} = 8$ TeV proton-proton collisions in the ATLAS detector," *Eur. Phys. J. C* **77** no. 4, (2017) 241, arXiv:1609.09324 [hep-ex].

[234] ATLAS Collaboration, "ATLAS data quality operations and performance for 2015–2018 data-taking," *JINST* **15** (2020) P04003, arXiv:1911.04632 [physics.ins-det].

[235] ATLAS Collaboration, "Selection of jets produced in 13 TeV proton–proton collisions with the ATLAS detector." ATLAS-CONF-2015-029, 2015. https://cds.cern.ch/record/2037702.

[236] N. Hartmann, "ahoi." https://gitlab.com/nikoladze/ahoi, 2018.

[237] **ATLAS** Collaboration, "Object-based missing transverse momentum significance in the ATLAS detector," Tech. Rep. ATLAS-CONF-2018-038, CERN, Geneva, Jul, 2018. https://cds.cern.ch/record/2630948.

[238] A. Roodman, "Blind analysis in particle physics," *eConf* **C030908** (2003) TUIT001, arXiv:physics/0312102.

[239] ATLAS Collaboration, "A method for the construction of strongly reduced representations of ATLAS experimental uncertainties and the application thereof to the jet energy scale." ATL-PHYS-PUB-2015-014, 2015. https://cds.cern.ch/record/2037436.

[240] J. Bellm *et al.*, "Herwig 7.0/Herwig++ 3.0 release note," *Eur. Phys. J.* **C76** no. 4, (2016) 196, arXiv:1512.01178 [hep-ph].

[241] ATLAS Collaboration, "Simulation of top-quark production for the ATLAS experiment at $\sqrt{s} = 13$ TeV." ATL-PHYS-PUB-2016-004, 2016. https://cds.cern.ch/record/2120417.

[242] S. Frixione, E. Laenen, P. Motylinski, C. White, and B. R. Webber, "Single-top hadroproduction in association with a $W$ boson," *JHEP* **07** (2008) 029, arXiv:0805.3067 [hep-ph].

[243] **ATLAS Collaboration** Collaboration, "SUSY July 2020 Summary Plot Update," Tech. Rep. ATL-PHYS-PUB-2020-020, CERN, Geneva, Jul, 2020. http://cds.cern.ch/record/2725258.

[244] G. Apollinari, I. Béjar Alonso, O. Brüning, M. Lamont, and L. Rossi, *High-Luminosity Large Hadron Collider (HL-LHC): Preliminary Design Report*. CERN Yellow Reports: Monographs. CERN, Geneva, 2015. https://cds.cern.ch/record/2116337.

[245] **LHC Reinterpretation Forum** Collaboration, W. Abdallah *et al.*, "Reinterpretation of LHC Results for New Physics: Status and Recommendations after Run 2," *SciPost Phys.* **9** no. 2, (2020) 022, arXiv:2003.07868 [hep-ph].

[246] ATLAS Collaboration, "RECAST framework reinterpretation of an ATLAS Dark Matter Search constraining a model of a dark Higgs boson decaying to two $b$-quarks." ATL-PHYS-PUB-2019-032, 2019. https://cds.cern.ch/record/2686290.

[247] K. Cranmer and I. Yavin, "RECAST: Extending the Impact of Existing Analyses," *JHEP* **04** (2011) 038, arXiv:1010.2506 [hep-ex].

[248] S. Ovyn, X. Rouby, and V. Lemaitre, "DELPHES, a framework for fast simulation of a generic collider experiment," arXiv:0903.2225 [hep-ph].

[249] A. Buckley, J. Butterworth, D. Grellscheid, H. Hoeth, L. Lonnblad, J. Monk, H. Schulz, and F. Siegert, "Rivet user manual," *Comput. Phys. Commun.* **184** (2013) 2803–2819, arXiv:1003.0694 [hep-ph].

[250] A. Buckley, D. Kar, and K. Nordström, "Fast simulation of detector effects in Rivet," *SciPost Phys.* **8** (2020) 025, arXiv:1910.01637 [hep-ph].

[251] D. Dercks, N. Desai, J. S. Kim, K. Rolbiecki, J. Tattersall, and T. Weber, "CheckMATE 2: From the model to the limit," *Comput. Phys. Commun.* **221** (2017) 383–418, arXiv:1611.09856 [hep-ph].

[252] M. Drees, H. Dreiner, D. Schmeier, J. Tattersall, and J. S. Kim, "CheckMATE: Confronting your Favourite New Physics Model with LHC Data," *Comput. Phys. Commun.* **187** (2015) 227–265, arXiv:1312.2591 [hep-ph].